Supporting Information for σ-Complexation as a Strategy for Designing Copper-Based Light Emitters

Yeong-Eun Kim, Jin Kim, Joon Woo Park, Kiyoung Park and Yunho Lee**

Department of Chemistry, Korea Advanced Institute of Science and Technology
Daejeon 34141, Republic of Korea

Contents

EXPERIMENTAL SECTION

General Considerations. All manipulations were carried out using standard Schlenk or glovebox techniques under a N_2 atmosphere. Unless otherwise noted, solvents were deoxygenated and dried by thoroughly sparging with Ar gas followed by passage through an activated alumina column. Non-halogenated solvents were tested with a standard purple solution of sodium benzophenone ketyl in tetrahydrofuran in order to confirm effective oxygen and moisture removal. All reagents were purchased from commercial vendors and used without further purification unless otherwise stated. PPPMe[1], $Si^{H}P_2$[2] and $Si^{D}P_2$[3] were prepared according to the literature procedures. Elemental analyses were carried out at the KAIST Research Analysis Center on a Thermo Scientific FLASH 2000 series instrument. Deuterated solvents were purchased from Cambridge Isotope Laboratories, Inc. or Euriso-top, degassed, and dried over activated 4 Å molecular sieves prior to use.

X-ray Crystallography. The diffraction data of **2a** and **3** were collected on a Bruker SMART 1000. The diffraction data of **1**, **2b**, **2c**, **4a**, **4b** and **4c** were collected on a Bruker D8 QUEST. A suitable size and quality of crystal was coated with Paratone-*N* oil and mounted on a MiTeGen MicroLoop. The data were collected with graphite-monochromated Mo Kα radiation (λ = 0.71073 Å) at 120 K. Cell parameters were determined and refined by the SMART program.[4] Data reduction was performed using SAINT software.[5] An empirical absorption correction was applied using the SADABS program.[6] The structures were solved by direct methods, and all non-hydrogen atoms were subjected to anisotropic refinement by full-matrix least squares on F^2 by using the SHELXTL/PC package.[7] Unless otherwise noted, hydrogen atoms were placed at their geometrically calculated positions and refined riding on the corresponding carbon atoms with isotropic thermal parameters. Full crystallographic details can be obtained free of charge from the Cambridge Crystallographic Data Center via www.ccdc.cam.ac.uk/data_request/cif (CCDC 1497439-1497446 for **1-4c**).

Spectroscopic Measurements. A Bruker 400 spectrometer was used to measure ^{1}H NMR spectra. The chemical shifts for ^{1}H NMR spectra are quoted in parts per million (ppm) referenced to residual solvent peaks. The following abbreviations are used to describe peak splitting patterns when appropriate: s = singlet, d = doublet, t = triplet, m = multiplet, dd = doublet of doublets, dt = doublet of triplets, br s = broad singlet. Coupling constants, *J*, are reported in hertz (Hz). ^{13}C

NMR spectra were recorded on a Bruker 400 spectrometer. ^{13}C NMR chemical shifts are reported in parts per million (ppm) referenced to internal solvent peaks. The *N* values corresponding to ½ [J_{AX}+$J_{A'X}$] are provided when virtual couplings are observed in the ^{13}C NMR spectra.[8,9] ^{29}Si NMR spectra were recorded on a Bruker 400 spectrometer and were decoupled by broad band proton decoupling. The chemical shifts for ^{29}Si NMR spectra are quoted in parts per million (ppm) referenced to external tetramethylsilane as 0.0 ppm. ^{31}P NMR spectra were recorded on a Bruker 400 spectrometer and were decoupled by broad band proton decoupling. The chemical shifts for ^{31}P NMR spectra are quoted in parts per million (ppm) referenced to external phosphoric acid as 0.0 ppm. UV-Vis spectra were measured using an Agilent Cary 60 UV-Vis spectrophotometer with a 1 cm two-window quartz spectrophotometer cell sealed with a screw-cap purchased from Hellma Analytics (117.100-QS) and a 1 cm four-window quartz spectrophotometer cell sealed with a Teflon-cap purchased from Starna Scientific (23/Q/10). Emission spectra were recorded on a Jobin Yvon Horiba Fluorolog F13-11 spectrofluorometer. Infrared spectra were recorded in KBr pellets with an Agilent 660-IR instrument. Frequencies are given in reciprocal centimeters (cm^{-1}) and only selected absorbances are reported.

Lifetime measurements. Lifetime measurements were measured using an Edinburgh Instruments FL920 fluorescence lifetime spectrometer. Analyte solutions for lifetime measurements were prepared in concentrations of less than 1×10^{-4} M, to give optical densities of near 0.1 or below. All samples were prepared under a N_2(g) atmosphere and sealed with a Teflon stopper. Absorption spectra were measured before and after recording lifetime measurements to ensure that no degradation took place.

Computational details. The initial geometries for the ($Si^{H}P_2$)Cu(Cbz) (**2a**) and ($PP^{Me}P$)Cu(Cbz) (**4a**) computational models were obtained from their corresponding X-ray crystal structures. All computations considered were performed using the ORCA 3.0.3 program package developed by Dr. Frank Neese[10] with the BP86 functional[11-13] and the Ahlrichs def2-SVP[14] basis set with the def2-SVP/C correlation auxiliary basis set[15] for all atoms except for Cu, which was treated with the Ahlrichs TZVP basis set.[16] The BP functional was chosen over the B3LYP functional[17-19] due to the latter notably overestimating the energies of major electronic transitions in the TD-DFT calculations performed using the Tamm-Dancoff approximation[20] within the ±3 Hartree orbital energy window (Fig. S7). Using the Ahlrichs def2-TZVP[14] basis set with the def2-TZVP/C

correlation auxiliary basis set[15] for all the atoms did not significantly improve the TD-DFT-computed electronic structures (Fig. S8) and thus the def2-SVP set for non-metal atoms was used for potential energy curve calculations. To assess the geometric and electronic structures of the excited states, the geometry optimization at the MLCT excited states were tried but not successfully converged because of nearly degenerate states. Thus, the corresponding triplet state was considered, assuming that the singlet and triplet MLCT excited states have a similar electron density distribution and thus a similar geometry. Based on this geometry analysis, the Cu-P stretch normal mode was chosen to obtain potential energy curves; a series of geometries were obtained by incrementally distorting the ground-state geometry along the Cu-P stretch normal modes, and on these geometries, single point and TDDFT calculations were performed. Then, the energies of correlated states were used to form the potential energy curves of the ground and MLCT excited states.

Synthesis of ($Si^{H}P_2$)CuCl (1). To a solution of $Si^{H}P_2$ (2.794 g, 6.489 mmol) in 100 mL of THF was added a solution of copper(I) chloride (0.611 g, 6.17 mmol) in 20 mL of MeCN. The resulting colorless solution was stirred for 2 hours at room temperature, and volatiles were removed under vacuum. The product ($Si^{H}P_2$)CuCl (**1**, 2.900 g, 5.476 mmol, 88.8%) was isolated as a white solid after washing with diethyl ether and drying under vacuum. ^{1}H NMR (400 MHz, C_6D_6) δ 7.58 – 7.52 (m, 2H, Ar-*H*), 7.10 – 7.05 (m, 4H, Ar-*H*), 7.04 – 6.80 (m, 2H, Ar-*H*), 6.87 – 6.82 (m, 1H, Si*H*), 2.61 – 2.53 (m, 2H, C*H*(CH_3)$_2$), 2.16 – 2.06 (m, 2H, C*H*(CH_3)$_2$), 1.42 (dd, *J* = 16.6, 7.0 Hz, 6H, CH(C*H*$_3$)$_2$), 1.16 (dd, *J* = 16.4, 6.8 Hz, 6H, CH(C*H*$_3$)$_2$), 1.00 (dd, *J* = 12.0, 6.8 Hz, 6H, CH(C*H*$_3$)$_2$), 0.78 (dd, *J* = 15.0, 7.0 Hz, 6H, CH(C*H*$_3$)$_2$), 0.49 (d, *J* = 3.2 Hz, 3H, SiC*H*$_3$). ^{13}C NMR (101 MHz, C_6D_6) δ 146.0 (virtual t, *N* = 18.2 Hz, Ar-*C*), 137.8 (virtual t, *N* = 11.1 Hz, Ar-*C*), 135.1 (virtual t, *N* = 14.1 Hz, Ar-*C*), 131.9 (s, Ar-*C*), 129.4 (s, Ar-*C*), 128.7 (s, Ar-*C*), 25.4 (virtual t, *N* = 10.6 Hz, *C*H(CH_3)$_2$), 22.5 (virtual t, *N* = 7.1 Hz, *C*H(CH_3)$_2$), 19.6 (virtual t, *N* = 5.6 Hz, CH(*C*H$_3$)$_2$), 19.4 (virtual d, *N* = 2.0 Hz, CH(*C*H$_3$)$_2$), 19.2 (virtual d, *N* = 3.0 Hz, CH(*C*H$_3$)$_2$), 16.8 (s, CH(*C*H$_3$)$_2$), –1.74 (virtual t, *N* = 4.5 Hz, Si*C*H$_3$). ^{29}Si NMR (79 MHz, C_6D_6) δ –31.5 (t, *J* = 18.1 Hz). ^{31}P NMR (162 MHz, C_6D_6) δ 16.0 (s). UV-vis [THF, nm (M^{-1} cm^{-1})]: 253 (7300), 287 (3000). IR (KBr pellet, cm^{-1}): $\nu_{Si\text{-}H}$ = 1980 (br s), ν_{Ar} = 1563. Anal. Calcd. for $C_{25}H_{40}CuP_2SiCl$: C, 56.70; H, 7.61. Found: C, 56.45; H, 7.62. X-ray quality crystals were grown by slow diffusion of pentane into a saturated benzene solution of **1** at room temperature.

Synthesis of (Si^DP_2)CuCl (1-D). To a solution of Si^DP_2 (89 mg, 0.21 mmol) in 6 mL of THF/MeCN (5:1) was added copper(I) chloride (19 mg, 0.19 mmol). The mixture was stirred for 1 hour at room temperature, resulting in a colorless solution. The mixture was filtered through Celite and volatiles were removed under vacuum. The resulting solid was dissolved in benzene (10 mL) and filtered through Celite. Volatiles were removed under vacuum. The product (Si^DP_2)CuCl (**1-D**, 0.056 g, 0.11 mmol, 56%) was isolated as a white solid after washing with diethyl ether and drying under vacuum. ^{1}H NMR (400 MHz, C_6D_6) δ 7.56 – 7.52 (m, 2H, Ar-*H*), 7.10 – 7.04 (m, 4H, Ar-*H*), 7.03 – 6.97 (m, 2H, Ar-*H*), 2.61 – 2.53 (m, 2H, C*H*(CH_3)$_2$), 2.16 – 2.06 (m, 2H, C*H*(CH_3)$_2$), 1.41 (dd, *J* = 16.6, 7.0 Hz, 6H, CH(C*H*$_3$)$_2$), 1.15 (dd, *J* = 16.4, 6.8 Hz, 6H, CH(C*H*$_3$)$_2$), 1.00 (dd, *J* = 12.2, 7.0 Hz, 6H, CH(C*H*$_3$)$_2$), 0.78 (dd, *J* = 15.0, 7.0 Hz, 6H, CH(C*H*$_3$)$_2$), 0.48 (d, *J* = 3.2 Hz, 3H, SiC*H*$_3$). ^{31}P NMR (162 MHz, C_6D_6) δ 16.0 (s).

Synthesis of (Si^HP_2)Cu(Cbz) (2a). To a solution of **1** (409 mg, 0.772 mmol) and carbazole (130 mg, 0.775 mmol) in 20 mL of THF, potassium hexamethyldisilazide (0.50 M in toluene, 1.60 mL, 0.80 mmol) was added dropwise at –35 °C with stirring, resulting in an immediate color change from colorless to pale yellow. After the mixture was warmed to room temperature and stirred for 2 hours, all volatiles were removed under vacuum. The resulting solid was dissolved in benzene (10 mL) and filtered through Celite. Volatiles were removed under vacuum. The product (Si^HP_2)Cu(Cbz) (**2a**, 395 mg, 0.599 mmol, 77.6%) was isolated as a white powder after washing with pentane and drying under vacuum. ^{1}H NMR (400 MHz, C_6D_6) δ 8.55 (d, *J* = 7.6 Hz, 2H, Ar-*H*), 7.96 (d, *J* = 8.1 Hz, 2H, Ar-*H*), 7.73 (t, *J* = 7.4 Hz, 2H, Ar-*H*), 7.56 (d, *J* = 7.5 Hz, 2H, Ar-*H*), 7.39 (t, *J* = 7.3 Hz, 2H, Ar-*H*), 7.12 – 7.07 (m, 4H, Ar-*H*), 7.02 – 6.98 (m, 2H, Ar-*H*), 6.76 – 6.70 (m, 1H, Si*H*), 2.15 – 2.06 (m, 2H, C*H*(CH_3)$_2$), 1.65 – 1.58 (m, 2H, C*H*(CH_3)$_2$), 0.97 (dd, *J* = 15.8, 7.0 Hz, 6H, CH(C*H*$_3$)$_2$), 0.84 (dd, *J* = 14.4, 7.2 Hz, 6H, CH(C*H*$_3$)$_2$), 0.77 – 0.71 (m, 9H, CH(C*H*$_3$)$_2$, SiC*H*$_3$), 0.49 (dd, *J* = 13.2, 6.8 Hz, 6H, CH(C*H*$_3$)$_2$). ^{13}C NMR (101 MHz, C_6D_6) δ 151.5 (s, Ar-*C*), 145.2 (s, Ar-*C*), 139.3 (s, Ar-*C*), 135.1 (virtual t, *N* = 7.1 Hz, Ar-*C*), 131.4 (s, Ar-*C*), 129.4 (s, Ar-*C*), 129.1 (s, Ar-*C*), 126.7 (s, Ar-*C*), 123.2 (s, Ar-*C*), 120.6 (s, Ar-*C*), 115.6 (s, Ar-*C*), 114.9 (s, Ar-*C*), 26.4 (virtual t, *N* = 10.6 Hz, *C*H(CH_3)$_2$), 23.4 (virtual t, *N* = 6.6 Hz, *C*H(CH_3)$_2$), 19.4 (virtual t, *N* = 5.1 Hz, CH(*C*H$_3$)$_2$), 19.3 (s, CH(*C*H$_3$)$_2$), 18.7 (virtual t, *N* = 3.5 Hz, CH(*C*H$_3$)$_2$), 17.2 (s, CH(*C*H$_3$)$_2$), –1.43 (s, Si*C*H$_3$). ^{29}Si NMR (79 MHz, C_6D_6) δ –27.0 (t, *J* = 16.4 Hz). ^{31}P NMR (162 MHz, C_6D_6) δ 15.2 (s). UV-vis [THF, nm (M^{-1} cm^{-1})]: 315 (7300), 337 (2200), 360 (sh, 2200), 372 (3000), 392 (3100). IR (KBr pellet, cm^{-1}): $\nu_{Si\text{-}H}$ = 1961 (br s), ν_{Ar} =

1620, 1580. Anal. Calcd. for $C_{37}H_{48}CuNP_2Si$: C, 67.30; H, 7.33; N, 2.12. Found: C, 67.20; H, 7.70; N, 1.97. X-ray quality crystals were grown by slow diffusion of pentane into a saturated benzene solution of **2a** at room temperature.

Synthesis of (Si^DP_2)Cu(Cbz) (2a-D). To a solution of **1-D** (56 mg, 0.11 mmol) and carbazole (18 mg, 0.11 mmol) in 5 mL of THF, potassium hexamethyldisilazide (0.50 M in toluene, 21 µL, 0.11 mmol) was added dropwise at –35 °C with stirring, resulting in an immediate color change from colorless to pale yellow. After the mixture was warmed and stirred for 1 hour at room temperature, all volatiles were removed under vacuum. The resulting solid was dissolved in benzene (5 mL) and filtered through Celite. Volatiles were removed under vacuum. The product (Si^DP_2)Cu(Cbz) (**2a-D**, 67 mg, 0.10 mmol, 95%) was isolated as a light yellow powder after washing with pentane and drying under vacuum. ^{1}H NMR (400 MHz, C_6D_6) δ 8.55 (d, *J* = 7.6 Hz, 2H, Ar-*H*), 7.96 (d, *J* = 8.1 Hz, 2H, Ar-*H*), 7.73 (t, *J* = 7.4 Hz, 2H, Ar-*H*), 7.56 (d, *J* = 7.5 Hz, 2H, Ar-*H*), 7.39 (t, *J* = 7.3 Hz, 2H, Ar-*H*), 7.12 – 7.07 (m, 4H, Ar-*H*), 7.02 – 6.98 (m, 2H, Ar-*H*), 2.15 – 2.06 (m, 2H, C*H*(CH_3)$_2$), 1.65 – 1.58 (m, 2H, C*H*(CH_3)$_2$), 0.97 (dd, *J* = 15.8, 7.0 Hz, 6H, CH(C*H*$_3$)$_2$), 0.84 (dd, *J* = 14.4, 7.2 Hz, 6H, CH(C*H*$_3$)$_2$), 0.78 – 0.70 (m, 9H, CH(C*H*$_3$)$_2$, SiC*H*$_3$), 0.49 (dd, *J* = 13.2, 6.8 Hz, 6H, CH(C*H*$_3$)$_2$). ^{31}P NMR (162 MHz, C_6D_6) δ 15.2 (s). IR (KBr pellet, cm^{-1}): ν_{Ar} = 1620, 1580.

Synthesis of (Si^HP_2)Cu(Cbz^{tBu}) (2b). To a solution of **1** (159 mg, 0.300 mmol) and 3,6-di-*tert*-butylcarbazole (114 mg, 0.400 mmol) in 10 mL of THF, potassium hexamethyldisilazide (0.50 M in toluene, 0.80 mL, 0.40 mmol) was added dropwise at –35 °C with stirring, resulting in an immediate color change from colorless to pale yellow. After the mixture was warmed and stirred for 2 hours at room temperature, all volatiles were removed under vacuum. The resulting solid was dissolved in benzene (5 mL) and filtered through Celite. Volatiles were removed under vacuum. The resulting solid was dissolved in a minimal amount of THF (~ 3 mL) and pentane (~ 25 mL) was layered on the top of the solution. The white crystals were formed after 2 days at room temperature. The supernatant was decanted off and the resulting crystals were washed with pentane. The product (Si^HP_2)Cu(Cbz^{tBu}) (**2b**, 164 mg, 0.212 mmol, 70.8%) was isolated as white crystals after drying under vacuum. ^{1}H NMR (400 MHz, C_6D_6) δ 8.68 (s, 2H, Ar-*H*), 7.92 – 7.87 (m, 2H, Ar-*H*), 7.82 – 7.78 (m, 2H, Ar-*H*), 7.61 – 7.55 (m, 2H, Ar-*H*), 7.11 – 7.08 (m, 4H, Ar-*H*), 7.01 – 6.98 (m, 2H, Ar-*H*), 6.80 – 6.73 (m, 1H, Si*H*), 2.14 – 2.08 (m, 2H, C*H*(CH_3)$_2$), 1.63 (s,

20H, C*H*$(CH_3)_2$, C(C*H*$_3)_3$), 1.02 (dd, *J* = 14.5, 6.8 Hz, 6H, CH(C*H*$_3)_2$), 0.88 – 0.82 (m, 9H, CH(C*H*$_3)_2$, SiC*H*$_3$), 0.74 (dd, *J* = 15.0, 6.6 Hz, 6H, CH(C*H*$_3)_2$), 0.49 (dd, *J* = 11.8, 6.6 Hz, 6H, CH(C*H*$_3)_2$). ^{13}C NMR (101 MHz, C_6D_6) δ 150.2 (s, Ar-*C*), 145.2 (virtual t, *N* = 18.6 Hz, Ar-*C*), 139.4 (virtual t, *N* = 10.6 Hz, Ar-*C*), 136.4 (s, Ar-*C*), 135.1 (virtual t, *N* = 7.3 Hz, Ar-*C*), 131.5 (s, Ar-*C*), 129.3 (s, Ar-*C*), 129.1 (s, Ar-*C*), 126.5 (s, Ar-*C*), 120.8 (s, Ar-*C*), 116.4 (s, Ar-*C*), 115.0 (s, Ar-*C*), 34.9 (s, *C*$(CH_3)_3$), 32.9 (s, C(*C*H$_3)_3$), 26.4 (virtual t, *N* = 10.1 Hz, *C*H$(CH_3)_2$), 23.4 (virtual t, *N* = 6.1 Hz, *C*H$(CH_3)_2$), 19.6 (virtual t, *N* = 5.1 Hz, CH(*C*H$_3)_2$), 19.4 (virtual t, *N* = 2.7 Hz, CH(*C*H$_3)_2$), 18.8 (virtual t, *N* = 3.7 Hz, CH(*C*H$_3)_2$), 17.2 (s, CH(*C*H$_3)_2$), –1.34 (virtual t, *N* = 5.1 Hz, Si*C*H$_3$). ^{29}Si NMR (79 MHz, C_6D_6) δ –27.0 (t, *J* = 15.8 Hz). ^{31}P NMR (162 MHz, C_6D_6) δ 15.3 (s). UV-vis [THF, nm (M^{-1} cm^{-1})]: 318 (9700), 342 (2700), 360 (sh, 2000), 378 (2700), 397 (2500). IR (KBr pellet, cm^{-1}): $\nu_{Si\text{-}H}$ = 1974 (br s), ν_{Ar} = 1627, 1591, 1563, 1560. Anal. Calcd. for $C_{45}H_{64}CuNP_2Si$: C, 69.96; H, 8.35; N, 1.81. Found: C, 69.69; H, 8.44; N, 1.75. X-ray quality crystals were grown by layering of pentane into a saturated THF solution of **2b** at room temperature.

Synthesis of (Si^HP_2)Cu(Cbz^I) (2c). To a solution of **1** (382 mg, 0.721 mmol) and 3,6-diiodocarbazole (308 mg, 0.736 mmol) in 20 mL of THF, potassium hexamethyldisilazide (0.50 M in toluene, 1.60 mL, 0.80 mmol) was added dropwise at –35 °C with stirring. The resulting colorless solution was warmed and stirred for 2 hours. After all volatiles were removed under vacuum, the resulting solid was dissolved in benzene (10 mL) and filtered through Celite. Volatiles were removed under vacuum. The product (Si^HP_2)Cu(Cbz^I) (**2c**, 401 mg, 0.440 mmol, 61.0%) was obtained as a light yellow powder after washing with diethyl ether and drying under vacuum. ^{1}H NMR (400 MHz, C_6D_6) δ 8.53 – 8.51 (m, 2H, Ar-*H*), 7.91 – 7.85 (m, 2H, Ar-*H*), 7.59 – 7.50 (m, 4H, Ar-*H*), 7.11 – 7.04 (m, 4H, Ar-*H*), 7.02 – 6.97 (m, 2H, Ar-*H*), 6.49 – 6.42 (m, 1H, Si*H*), 2.06 – 1.97 (m, 2H, C*H*$(CH_3)_2$), 1.57 – 1.50 (m, 2H, C*H*$(CH_3)_2$), 0.84 (dd, *J* = 15.8, 7.0 Hz, 6H, CH(C*H*$_3)_2$), 0.77 (dd, *J* = 14.4, 7.2 Hz, 6H, CH(C*H*$_3)_2$), 0.68 (d, J = 3.2 Hz, 3H, SiC*H*$_3$), 0.61 (dd, *J* = 16.2, 7.0 Hz, 6H, CH(C*H*$_3)_2$), 0.42 (dd, *J* = 13.6, 6.8 Hz, 6H, CH(C*H*$_3)_2$). ^{13}C NMR (101 MHz, C_6D_6) δ 150.0 (s, Ar-*C*), 144.7 (virtual t, *N* = 18.43 Hz, Ar-*C*), 138.8 (virtual t, *N* = 11.2 Hz, Ar-*C*), 135.1 (virtual t, *N* = 7.2 Hz, Ar-*C*), 131.5 (s, Ar-*C*), 129.6 (s, Ar-*C*), 129.5 (s, Ar-*C*), 129.3 (s, Ar-*C*), 128.6 (s, Ar-*C*), 128.5 (s, Ar-*C*), 117.9 (s, Ar-*C*), 77.3 (s, Ar-*C*), 26.3 (virtual t, *N* = 10.0 Hz, *C*H$(CH_3)_2$), 23.3 (virtual t, *N* = 6.5 Hz, *C*H$(CH_3)_2$), 19.4 (virtual t, *N* = 4.9 Hz, CH(*C*H$_3)_2$), 19.2 (virtual t, *N* = 2.4 Hz, CH(*C*H$_3)_2$), 18.6 (virtual t, *N* = 3.7

Hz, CH(CH_3)$_2$), 17.2 (s, CH(CH_3)$_2$), –1.59 (virtual t, N = 4.5 Hz, SiCH_3). ^{29}Si NMR (79 MHz, THF/C_6D_6) δ –26.8 (t, J = 16.2 Hz). ^{31}P NMR (162 MHz, C_6D_6) δ 15.4 (s). UV-vis [THF, nm (M^{-1} cm^{-1})]: 325 (sh, 13400), 353 (sh, 4400), 369 (2600), 389 (3200), 410 (2900). IR (KBr pellet, cm^{-1}): $\nu_{Si\text{-}H}$ = 1981 (br s), ν_{Ar} = 1610. Anal. Calcd. for $C_{37}H_{46}CuI_2NP_2Si$: C, 48.72; H, 5.08; N, 1.54. Found: C, 48.71; H, 5.09; N, 1.52. X-ray quality crystals were grown by slow diffusion of pentane into a saturated THF solution of **2c** at room temperature.

Synthesis of (PP^{Me}P)CuCl (3). To a solution of PP^{Me}P (781 mg, 1.81 mmol) in 5 mL of THF was added copper(I) chloride (178 mg, 1.80 mmol). The resulting yellow suspension was stirred for 1 hour at room temperature. Volatiles were removed under vacuum. The product (PP^{Me}P)CuCl (**3**, 908 mg, 1.71 mmol, 95.0%) was isolated as a yellow powder after washing with pentane and drying under vacuum. ^{1}H NMR (400 MHz, C_6D_6) δ 7.56 – 7.52 (m, 2H, Ar-*H*), 7.13 – 7.10 (m, 2H, Ar-*H*), 7.06 – 7.02 (m, 2H, Ar-*H*), 7.00 – 6.96 (m, 2H, Ar-*H*), 2.50 – 2.43 (m, 2H, C*H*(CH_3)$_2$), 2.16 – 2.09 (m, 2H, C*H*(CH_3)$_2$), 1.55 – 1.49 (m, 9H, PCH_3, C*H*(CH_3)$_2$), 1.15 – 1.06 (m, 12H, CH(CH_3)$_2$), 0.73 (dd, J = 14.4, 7.0 Hz, 6H, CH(CH_3)$_2$). ^{13}C NMR (101 MHz, C_6D_6) δ 146.8 (virtual t, N = 17.2 Hz, Ar-*C*), 141.0 – 140.2 (m, Ar-*C*), 131.9 (s, Ar-*C*), 131.8 (s, Ar-*C*), 131.4 (virtual t, N = 4.1 Hz, Ar-*C*), 129.9 (s, Ar-*C*), 129.2 (s, Ar-*C*), 27.0 (virtual t, N = 8.1 Hz, *C*H(CH_3)$_2$), 22.9 (virtual d, N = 15.6 Hz, *C*H(CH_3)$_2$), 19.9 – 19.8 (m, CH(CH_3)$_2$), 19.6 (s, CH(CH_3)$_2$), 17.5 (s, CH(CH_3)$_2$), 12.8 – 12.5 (m, PCH_3). ^{31}P NMR (162 MHz, C_6D_6) δ 22.6 (br s, 2P), –36.6 (br s, 1P). Anal. Calcd. for $C_{25}H_{39}ClCuP_3$: C, 56.49; H, 7.40. Found: C, 56.54; H, 7.47. X-ray quality crystals were grown by slow diffusion of pentane into a saturated THF solution of **3** at room temperature.

Synthesis of (PP^{Me}P)Cu(Cbz) (4a). To a solution of **3** (213 mg, 0.400 mmol) and carbazole (70 mg, 0.40 mmol) in 10 mL of THF, potassium hexamethyldisilazide (0.50 M in toluene, 0.80 mL, 0.40 mmol) was added dropwise at –35 °C with stirring, resulting in an immediate color change from yellow to orange. The mixture was warmed to room temperature and stirred for 1 hour. After the mixture was filtered through Celite, volatiles were removed under vacuum. The product (PP^{Me}P)Cu(Cbz) (**4a**, 233 mg, 0.352 mmol, 88%) was isolated as a yellow powder after washing with pentane and drying under vacuum. ^{1}H NMR (400 MHz, C_6D_6) δ 8.59 – 8.54 (m, 2H, Ar-*H*), 8.34 – 8.28 (m, J = 8.0 Hz, 1H, Ar-*H*), 7.83 – 7.72 (m, 2H, Ar-*H*), 7.68 – 7.64 (m, 1H, Ar-*H*), 7.63 – 7.57 (m, 2H, Ar-*H*), 7.46 – 7.41 (m, 1H, Ar-*H*), 7.39 – 7.33 (m, 1H, Ar-*H*), 7.11 –

7.03 (m, 4H, Ar-*H*), 6.99 – 6.93 (m, 2H, Ar-*H*), 2.18 – 2.06 (m, 2H, C*H*(CH_3)$_2$), 1.88 (s, 3H, PCH_3), 1.64 – 1.55 (m, 2H, C*H*(CH_3)$_2$), 1.19 (dd, *J* = 15.8, 7.0 Hz, 6H, CH(CH_3)$_2$), 0.79 (dd, *J* = 14.2, 7.0 Hz, 6H, CH(CH_3)$_2$), 0.64 (dd, *J* = 16.2, 7.0 Hz, 6H, CH(CH_3)$_2$), 0.45 (dd, *J* = 12.6, 7.0 Hz, 6H, CH(CH_3)$_2$). ^{13}C NMR (101 MHz, C_6D_6) δ 152.9 (s, Ar-*C*), 151.9 (s, Ar-*C*), 146.1 (virtual dt, *N* = 24.8, 18.0 Hz, Ar-*C*), 141.1 (virtual dt, *N* = 37.2, 15.1 Hz, Ar-*C*), 131.7 (d, *J* = 10.2 Hz, Ar-*C*), 131.3 (virtual t, *N* = 4.0 Hz, Ar-*C*), 130.0 (d, *J* = 3.0 Hz, Ar-*C*), 129.5 (s, Ar-*C*), 126.6 (d, *J* = 18.8 Hz, Ar-*C*), 123.3 (s, Ar-*C*), 122.5 (s, Ar-*C*), 120.4 (s, Ar-*C*), 116.5 (s, Ar-*C*), 115.6 (s, Ar-*C*), 114.7 (s, Ar-*C*), 114.4 (s, Ar-*C*), 27.1 (virtual t, *N* = 7.6 Hz, C*H*(CH_3)$_2$), 23.8 (d, *J* = 14.0 Hz, *C*H(CH_3)$_2$), 20.1 (virtual t, *N* = 6.3 Hz, CH(*C*H_3)$_2$), 19.8 (virtual t, *N* = 3.3 Hz, CH(*C*H_3)$_2$), 19.2 (s, CH(*C*H_3)$_2$), 17.5 (s, CH(*C*H_3)$_2$), 14.9 (virtual t, *N* = 11.6 Hz, P*C*H_3). ^{31}P NMR (162 MHz, C_6D_6) δ 21.1 (d, *J* = 132.7 Hz, 2P), –29.4 (t, *J* = 130.8 Hz, 1P). UV-vis [THF, nm (M^{-1} cm^{-1})]: 316 (9800), 374 (4300), 394 (4000). Anal. Calcd. for $C_{37}H_{47}CuNP_3$: C, 67.10; H, 7.15; N, 2.12. Found: C, 66.85; H, 7.11; N, 2.00. X-ray quality crystals were grown by slow diffusion of pentane into a saturated THF solution of **4a** at room temperature.

Synthesis of (PP^{Me}P)Cu(Cbz^{tBu}) (4b). To a solution of **3** (213 mg, 0.400 mmol) and 3,6-di-*tert*-butylcarbazole (114 mg, 0.400 mmol) in 10 mL of THF, potassium hexamethyldisilazide (0.50 M in toluene, 0.80 mL, 0.40 mmol) was added dropwise at –35 °C with stirring, resulting in a yellow solution. The solution was warmed and stirred for 1 hour at room temperature. The mixture was filtered through Celite and all volatiles were removed under vacuum. The product (PP^{Me}P)Cu(Cbz^{tBu}) (**4b**, 291 mg, 0.376 mmol, 94%) was isolated as a yellow powder after washing with pentane and drying under vacuum. ^{1}H NMR (400 MHz, C_6D_6) δ 8.70 – 8.66 (m, 2H, Ar-*H*), 8.25 – 8.20 (m, 1H, Ar-*H*), 7.90 – 7.85 (m, 1H, Ar-*H*), 7.76 – 7.72 (m, 1H, Ar-*H*), 7.69 – 7.66 (m, 1H, Ar-*H*), 7.64 – 7.59 (m, 2H, Ar-*H*), 7.10 – 7.05 (m, 4H, Ar-*H*), 6.99 – 6.94 (m, 2H, Ar-H), 2.17 – 2.07 (m, 2H, C*H*(CH_3)$_2$), 1.94 (s, 3H, PCH_3), 1.70 – 1.56 (m, 20H, C(CH_3)$_3$, C*H*(CH_3)$_2$), 1.22 (dd, *J* = 15.8, 7.0 Hz, 6H, CH(CH_3)$_2$), 0.80 (dd, *J* = 13.8, 7.0 Hz, 6H, CH(CH_3)$_2$), 0.64 (dd, *J* = 16.4, 6.8 Hz, 6H, CH(CH_3)$_2$), 0.43 (dd, *J* = 12.8, 6.8 Hz, 6H, CH(CH_3)$_2$). ^{13}C NMR (101 MHz, C_6D_6) δ 151.6 (s, Ar-*C*), 120.7 (s, Ar-*C*), 146.5 – 146.0 (m, Ar-*C*), 141.4 – 141.0 (m, Ar-*C*), 136.2 (s, Ar-*C*), 135.8 (s, Ar-*C*), 131.7 (d, *J* = 10.2 Hz, Ar-*C*), 131.3 (virtual t, *N* = 4.6 Hz, Ar-*C*), 129.9 (s, Ar-*C*), 129.4 (s, Ar-*C*), 126.4 (d, *J* = 13.6 Hz, Ar-*C*), 120.9 (s, Ar-*C*), 120.1 (s, Ar-*C*), 116.2 (s, Ar-*C*), 115.7 (s, Ar-*C*), 114.9 (s, Ar-*C*), 34.9 (d, *J* = 8.8 Hz, *C*H(CH_3)$_2$), 33.0 (d, *J* = 7.0 Hz, *C*(CH_3)$_3$), 27.1 (virtual t, *N* = 7.6 Hz, *C*H(CH_3)$_2$), 23.8 (d,

J = 14.2 Hz, CH(CH$_3$)$_2$), 20.2 (virtual t, N = 6.4 Hz, CH(CH$_3$)$_2$), 19.8 (virtual t, N = 3.7 Hz, CH(CH$_3$)$_2$), 19.3 (s, CH(CH$_3$)$_2$), 17.5 (s, C(CH$_3$)$_3$), 15.0 (virtual t, N = 12.1 Hz, PCH$_3$). ^{31}P NMR (162 MHz, C_6D_6) δ 21.2 (d, J = 131.4 Hz, 2P), –29.3 (t, J = 132.2 Hz, 1P). UV-vis [THF, nm (M^{-1} cm^{-1})]: 319 (10800), 379 (4100), 398 (3600). Anal. Calcd. for $C_{45}H_{63}CuNP_3$: C, 69.79; H, 8.20; N, 1.81. Found: C, 69.62; H, 8.16; N, 1.84. X-ray quality crystals were grown by slow diffusion of pentane into a saturated THF solution of **4b** at room temperature.

Synthesis of (PP^{Me}P)Cu(Cbz^{I}) (4c). To a solution of **3** (213 mg, 0.400 mmol) and 3,6-diiodocarbazole (171 mg, 0.400 mmol) in 10 mL of THF, potassium hexamethyldisilazide (0.50 M in toluene, 0.80 mL, 0.40 mmol) was added dropwise at –35 °C with stirring, resulting in an immediate color change from yellow to red-orange. The solution was warmed and stirred for 1 hour at room temperature. The mixture was filtered through Celite and volatiles were removed under vacuum. The product (PP^{Me}P)Cu(Cbz^{I}) (**4c**, 216 mg, 0.236 mmol, 59%) was isolated as a yellow powder after washing with pentane and drying under vacuum. ^{1}H NMR (400 MHz, C_6D_6) δ 8.56 – 8.51 (m, 2H, Ar-H), 8.00 – 7.92 (m, 2H, Ar-H), 7.82 – 7.77 (m, 1H, Ar-H), 7.58 – 7.53 (m, 2H, Ar-H), 7.34 – 7.30 (m, 1H, Ar-H), 7.09 – 7.01 (m, 4H, Ar-H), 6.99 – 6.93 (m, 2H, Ar-H), 2.09 – 1.98 (m, 2H, CH(CH$_3$)$_2$), 1.74 (s, 3H, PCH_3), 1.55 – 1.46 (m, 2H, CH(CH$_3$)$_2$), 1.04 (dd, J = 16.0, 6.8 Hz, 6H, CH(CH_3)$_2$), 0.71 (dd, J = 14.4, 7.2 Hz, 6H, CH(CH_3)$_2$), 0.52 (dd, J = 16.2, 7.0 Hz, 6H, CH(CH_3)$_2$), 0.38 (dd, J = 12.8, 7.2 Hz, 6H, CH(CH_3)$_2$). ^{13}C NMR (101 MHz, C_4D_8O)[21] δ 151.9 (d, J = 5.2 Hz, Ar-C), 151.0 (s, Ar-C), 146.5 (virtual dt, N = 26.3, 17.7 Hz, Ar-C), 141.7 – 141.0 (m, Ar-C), 132.8 (s, Ar-C), 132.7 (s, Ar-C), 132.6 (d, J = 4.6 Hz, Ar-C), 132.1 (s, Ar-C), 131.5 (s, Ar-C), 131.4 (d, J = 3.1 Hz, Ar-C), 130.8 (s, Ar-C), 129.2 (s, Ar-C), 129.0 (d, J = 3.7 Hz, Ar-C), 128.2 (d, J = 12.8 Hz, Ar-C), 119.5 (s, Ar-C), 118.8 (d, J = 6.4 Hz, Ar-C), 77.0 (s, Ar-C), 76.6 (s, Ar-C), 28.1 (virtual t, N = 8.8 Hz, CH(CH$_3$)$_2$), 24.8 (dd, J = 16.4, 2.9 Hz, CH(CH$_3$)$_2$), 20.8 (virtual t, N = 6.1 Hz, CH(CH$_3$)$_2$), 20.4 (virtual t, N = 3.2 Hz, CH(CH$_3$)$_2$), 19.6 (d, J = 6.4 Hz, CH(CH$_3$)$_2$), 18.2 (s, CH(CH$_3$)$_2$), 15.2 (virtual t, N = 10.7 Hz, PCH$_3$). ^{31}P NMR (162 MHz, C_6D_6) δ 21.3 (d, J = 129.7 Hz, 2P), –29.3 (t, J = 129.4 Hz, 1P). UV-vis [THF, nm (M^{-1} cm^{-1})]: 315 (14400), 390 (sh, 3300), 408 (1800). Anal. Calcd. for $C_{37}H_{45}CuI_2NP_3$: C, 48.62; H, 4.96; N, 1.53. Found: C, 48.75; H, 4.95; N, 1.53. X-ray quality crystals were grown by slow diffusion of pentane into a saturated THF solution of **4c** at room temperature.

Quantum yield experiments. Analyte solutions in either tetrahydrofuran (n = 1.405)[22] or toluene (n = 1.496)[22] were prepared in concentrations of 1×10^{-4} M or less, to give optical densities of near 0.1 or below. All samples were prepared under a N_2(g) atmosphere and sealed with a Teflon stopper. Absorption spectra were measured before and after recording lifetime measurements to ensure that no degradation took place. A solution of perylene in ethanol was prepared in a N_2 charged glove box with the optical density of ca. 0.01 at 392 nm and 397 nm. Emission spectra were measured with excitations of 392 nm or 397 nm at 298 K. Quantum yields were calculated using following the literature method.[23] The standard sample of perylene in ethanol with a quantum yield of 0.93 was utilized as a reference.[24]

Complex	λ_{ex} (nm)	O.D. at λ_{ex}	I (counts)	Φ (calc.)
	392 nm	0.013780	694944410	
		0.118482	1321774990	0.41
2a		0.111360	1165283680	0.38
(in THF)		0.091417	993110370	0.40
				0.40 (avg.)
standard	392 nm	0.013780	694944410	
2a (in toluene)		0.074811	197418350	0.10
standard	392 nm	0.013780	694944410	
		0.117140	1099381210	0.34
2a-D (in THF)		0.097689	948367710	0.35
				0.34 (avg.)
standard	397 nm	0.016089	865832270	
		0.092128	1629264940	0.61
2b		0.093170	1612007500	0.59
(in THF)		0.105099	1764839890	0.57
				0.59 (avg.)
standard	397 nm	0.016089	865832270	
2c		0.068375	8019130	< 0.01*
(in THF)		0.075024	8083350	< 0.01*
standard	392 nm	0.013780	694944410	
4a		0.074472	4591350	< 0.01*
(in THF)		0.117424	4436460	< 0.01*
standard	397 nm	0.016089	865832270	
4b		0.108303	6222040	< 0.01*
(in THF)		0.109227	6928190	< 0.01*

* Due to the low emission property, the background emission affects the quantum yield.

Figure S1. ^{1}H NMR spectrum (C_6D_6, 400 MHz) of ($Si^{H}P_2$)CuCl (**1**) at room temperature.

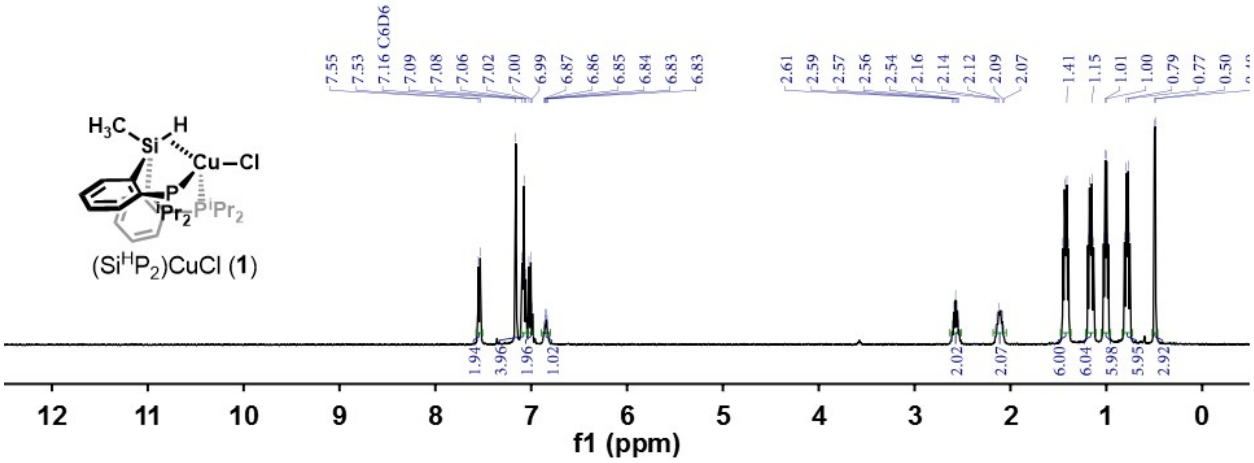

Figure S2. ^{13}C NMR spectrum (C_6D_6, 101 MHz) of ($Si^{H}P_2$)CuCl (**1**) at room temperature.

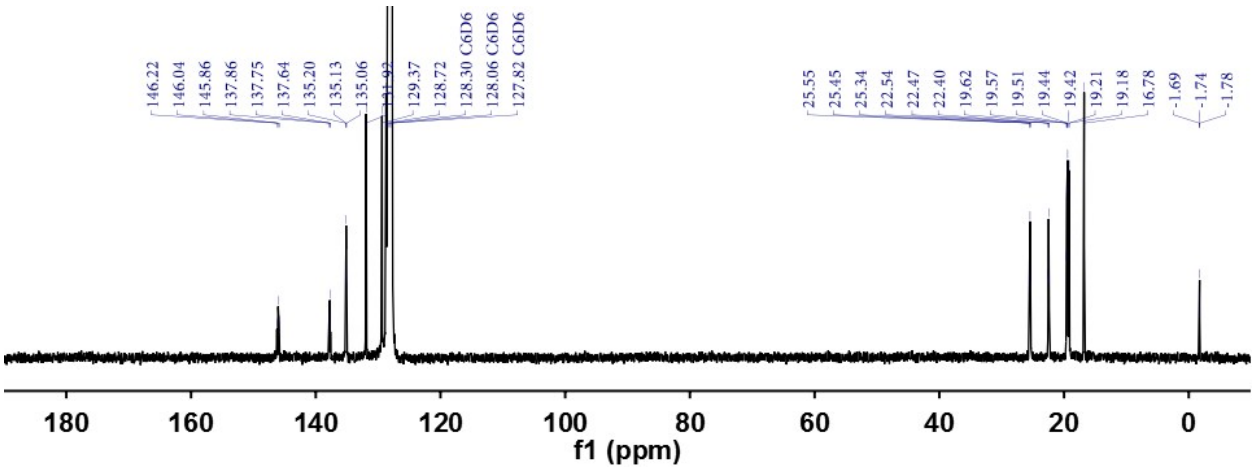

Figure S3. ^{29}Si NMR spectrum (C_6D_6, 79 MHz) of ($Si^{H}P_2$)CuCl (**1**) at room temperature.

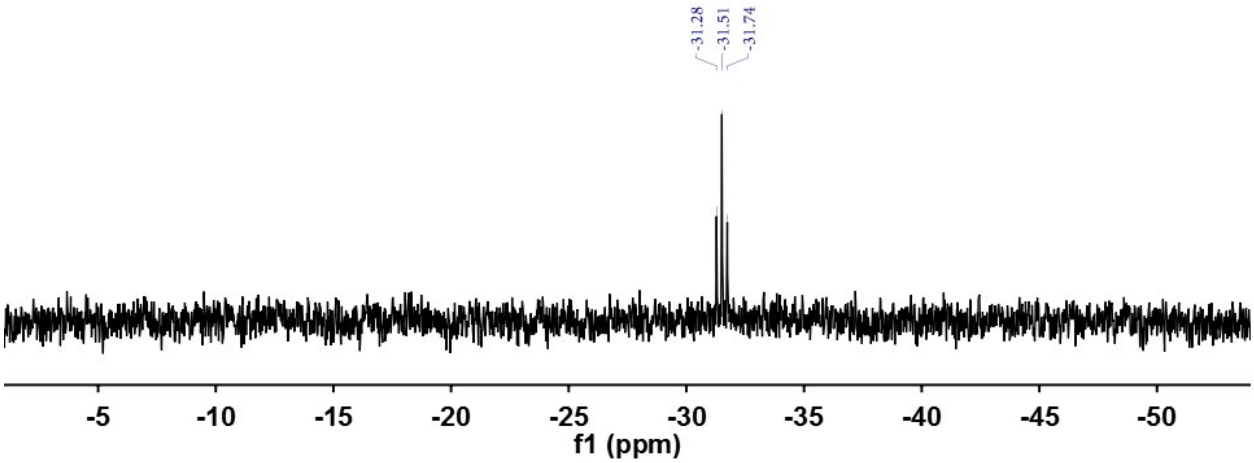

Figure S4. ^{31}P NMR spectrum (C_6D_6, 162 MHz) of ($Si^{H}P_2$)CuCl (**1**) at room temperature.

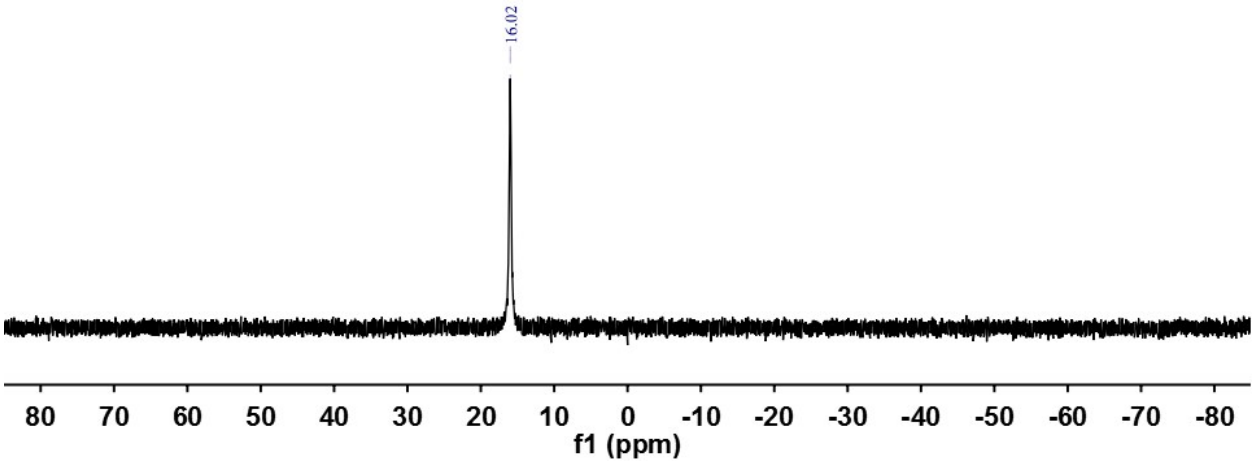

Figure S5. ^{1}H NMR spectrum (C_6D_6, 400 MHz) of ($Si^{D}P_2$)CuCl (**1-D**) at room temperature.

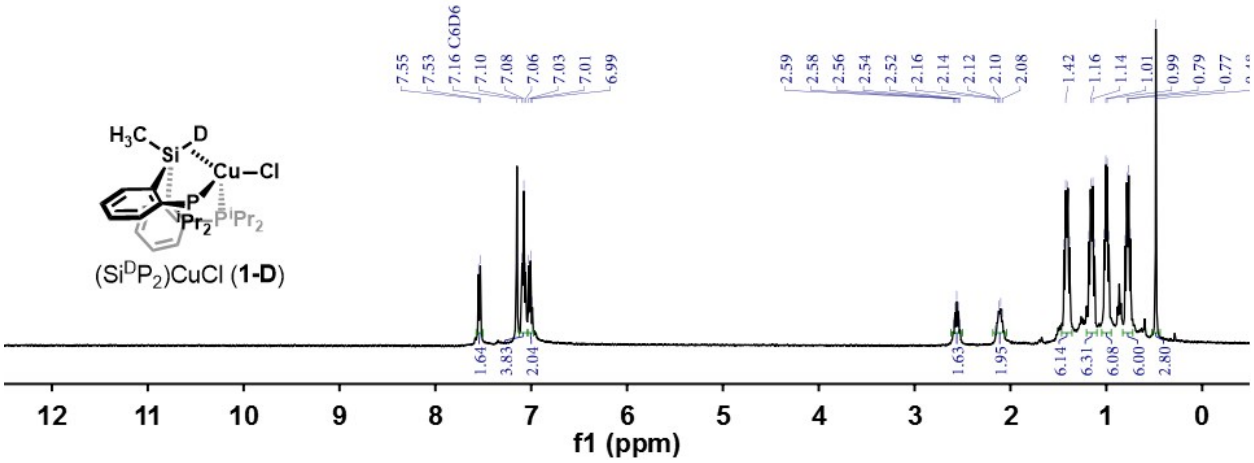

Figure S6. ^{31}P NMR spectrum (C_6D_6, 162 MHz) of ($Si^{D}P_2$)CuCl (**1-D**) at room temperature.

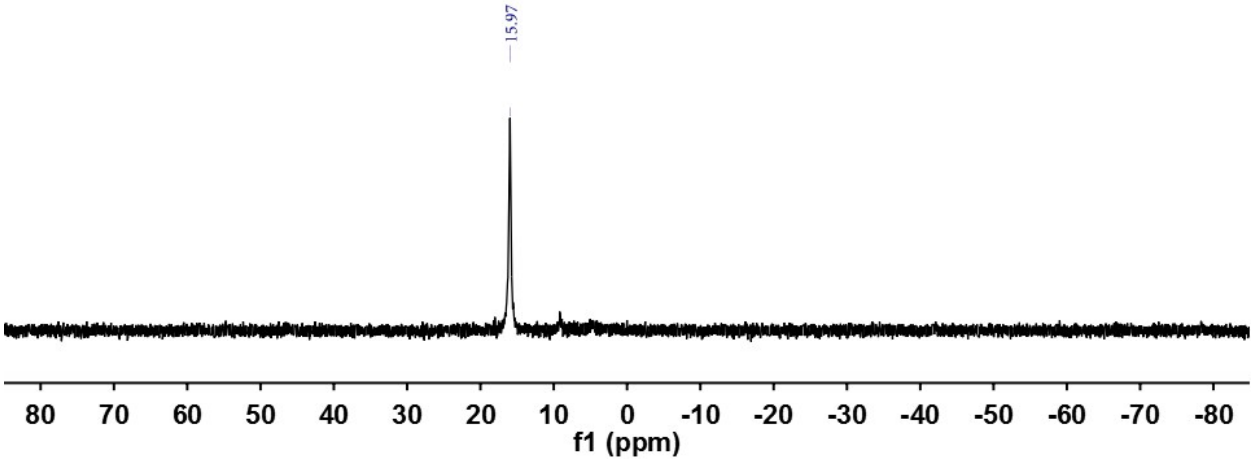

Figure S7. ^{1}H NMR spectrum (C_6D_6, 400 MHz) of ($Si^{H}P_2$)Cu(Cbz) (**2a**) at room temperature.

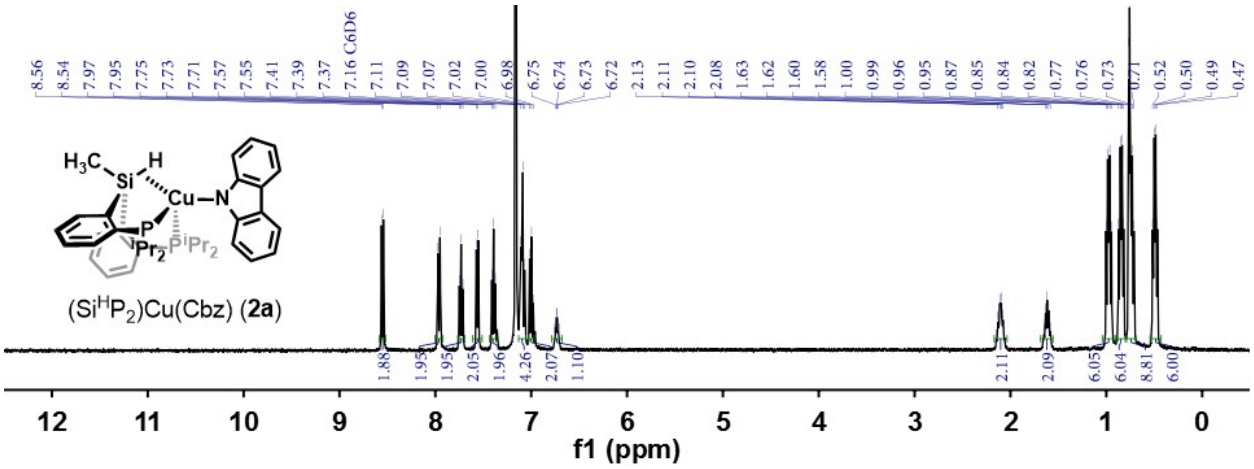

Figure S8. ^{13}C NMR spectrum (C_6D_6, 101 MHz) of ($Si^{H}P_2$)Cu(Cbz) (**2a**) at room temperature.

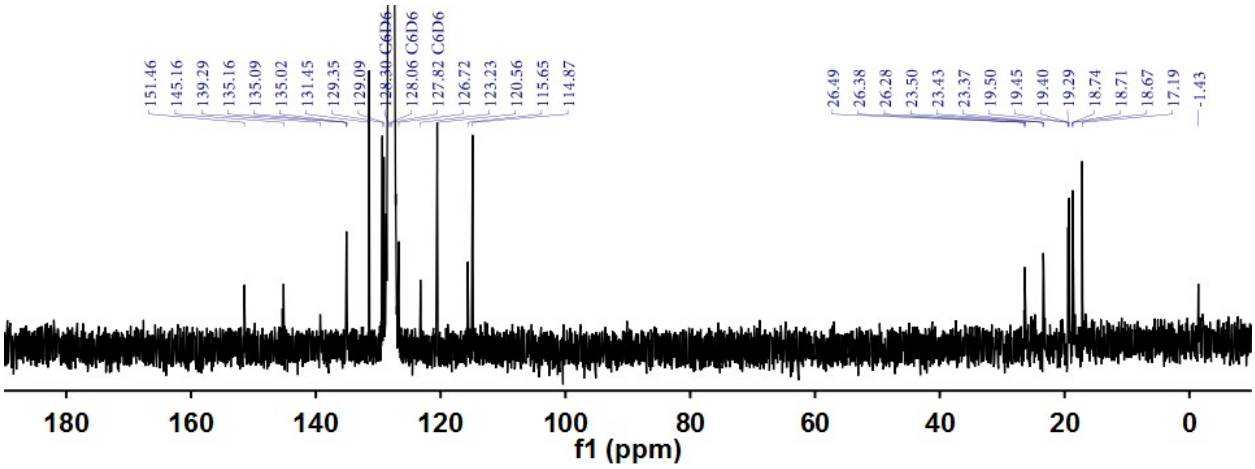

Figure S9. ^{29}Si NMR spectrum (C_6D_6, 79 MHz) of ($Si^{H}P_2$)Cu(Cbz) (**2a**) at room temperature.

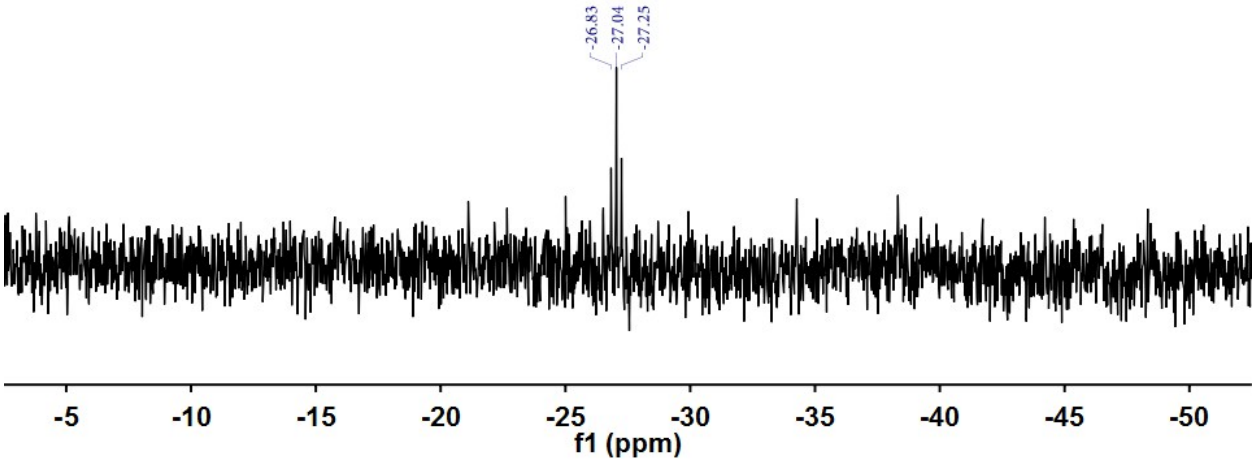

Figure S10. ^{31}P NMR spectrum (C_6D_6, 162 MHz) of ($Si^{H}P_2$)Cu(Cbz) (**2a**) at room temperature.

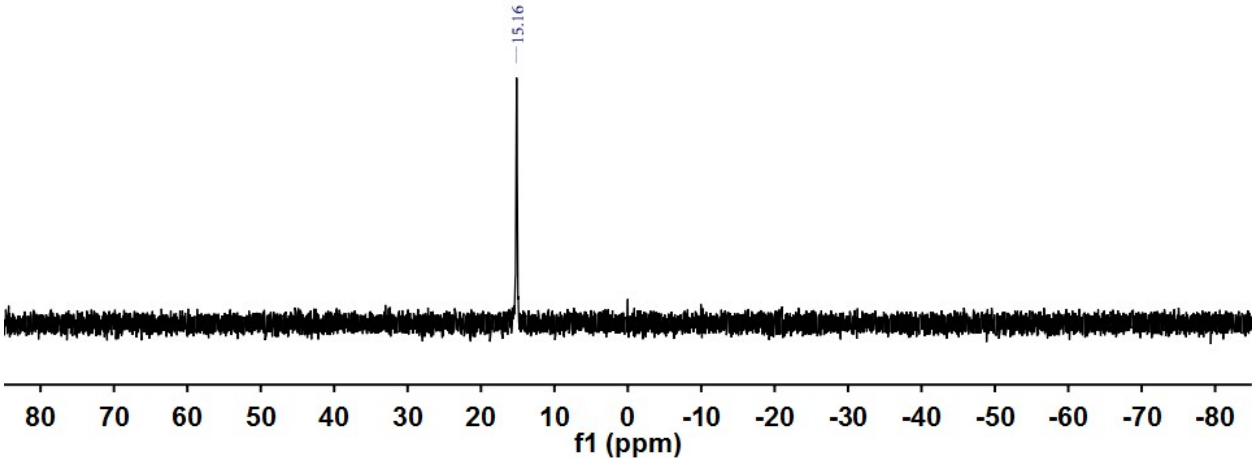

Figure S11. ^{1}H NMR spectrum (C_6D_6, 400 MHz) of ($Si^{D}P_2$)Cu(Cbz) (**2a-D**) at room temperature.

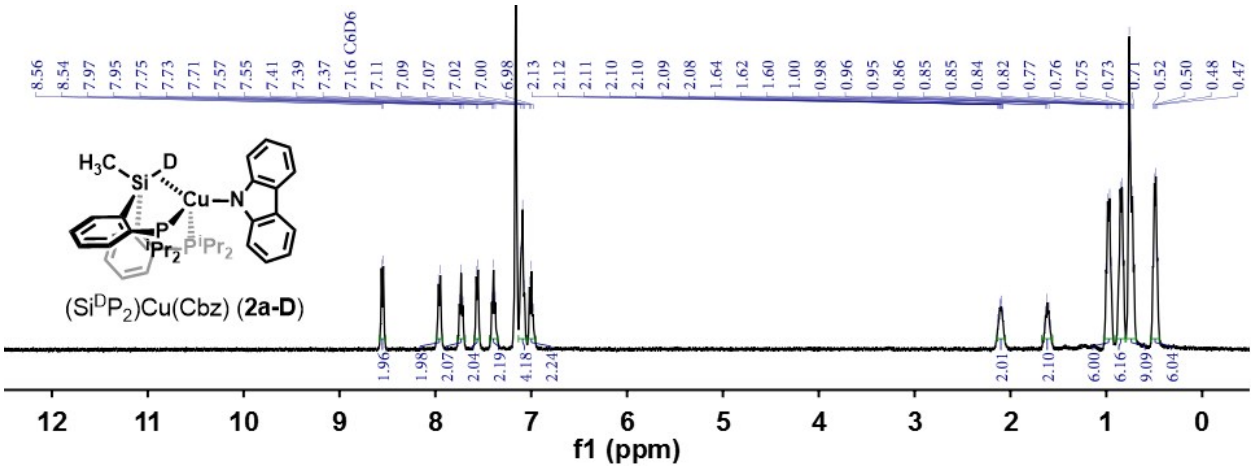

Figure S12. ^{31}P NMR spectrum (C_6D_6, 162 MHz) of ($Si^{D}P_2$)Cu(Cbz) (**2a-D**) at room temperature.

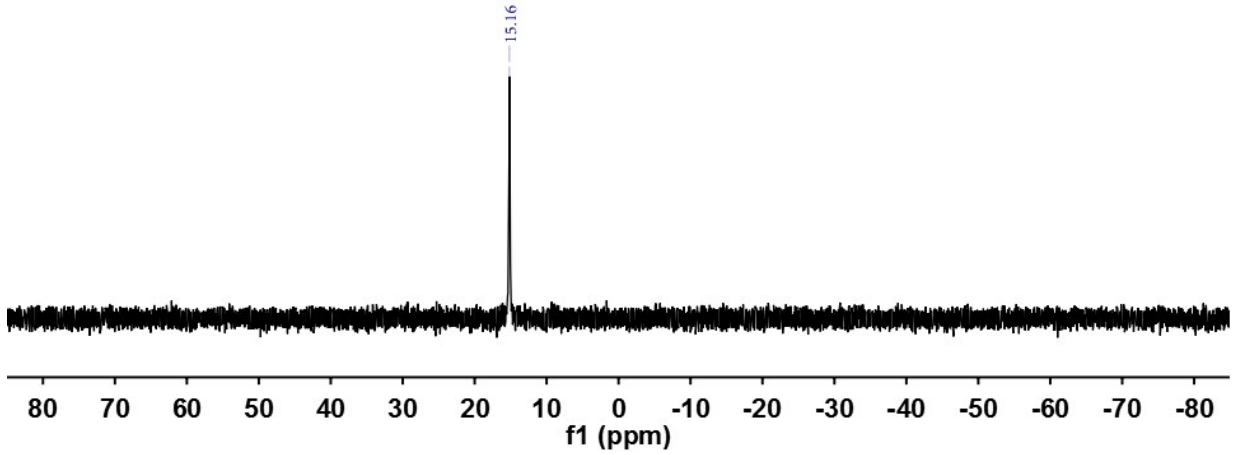

Figure S13. ^{1}H NMR spectrum (C_6D_6, 400 MHz) of ($Si^{H}P_2$)Cu(Cbz^{t}Bu) (**2b**) at room temperature.

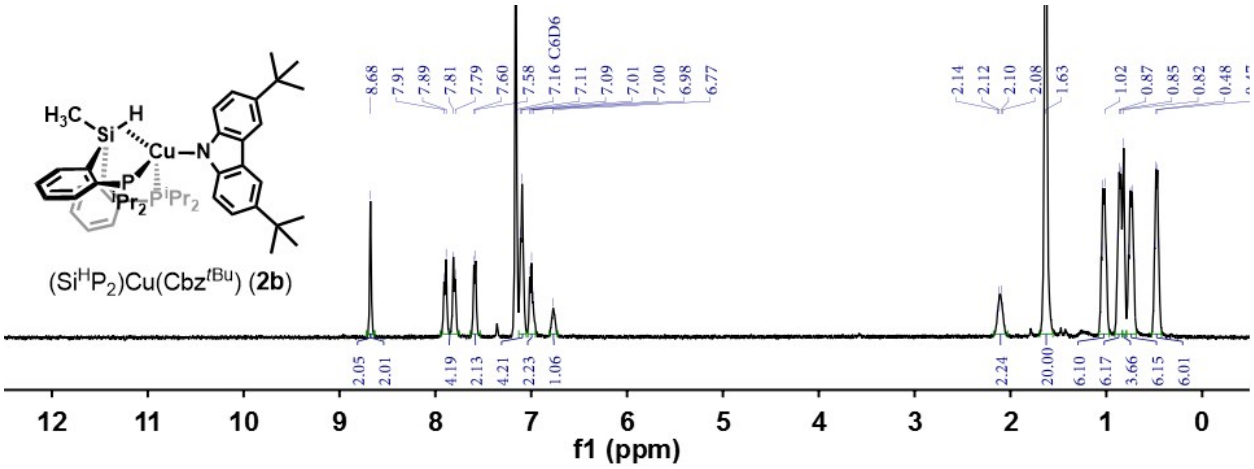

Figure S14. ^{13}C NMR spectrum (C_6D_6, 101 MHz) of ($Si^{H}P_2$)Cu(Cbz^{t}Bu) (**2b**) at room temperature.

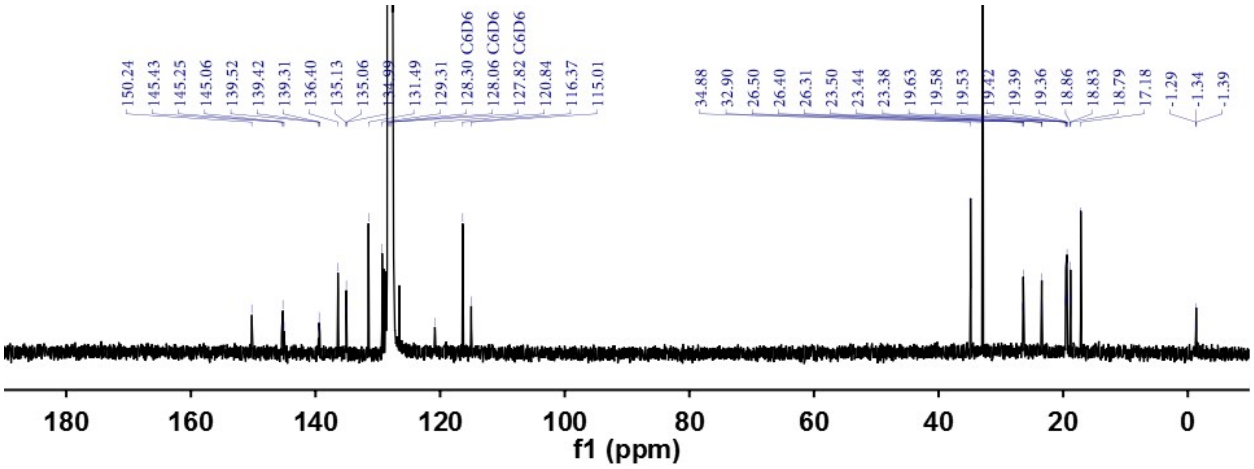

Figure S15. ^{29}Si NMR spectrum (C_6D_6, 79 MHz) of ($Si^{H}P_2$)Cu(Cbz^{t}Bu) (**2b**) at room temperature.

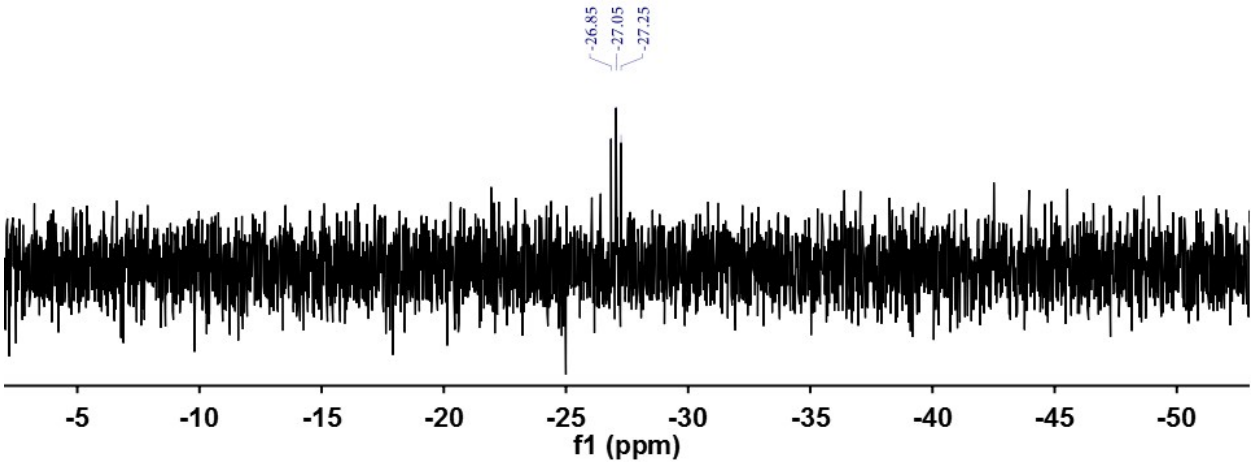

Figure S16. ^{31}P NMR spectrum (C_6D_6, 162 MHz) of (Si^HP_2)Cu(Cbz^{tBu}) (**2b**) at room temperature.

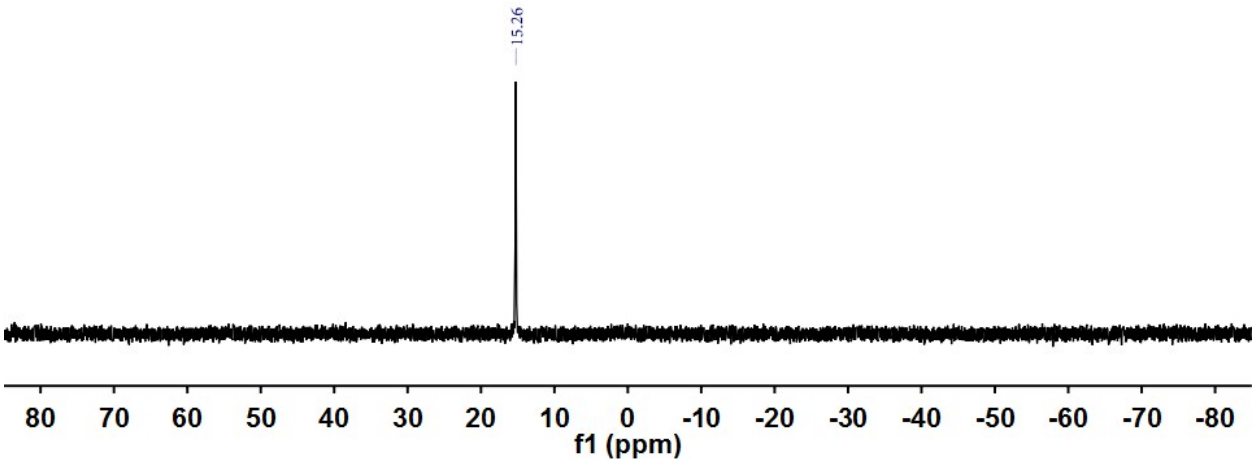

Figure S17. ^1H NMR spectrum (C_6D_6, 400 MHz) of (Si^HP_2)Cu(Cbz^I) (**2c**) at room temperature.

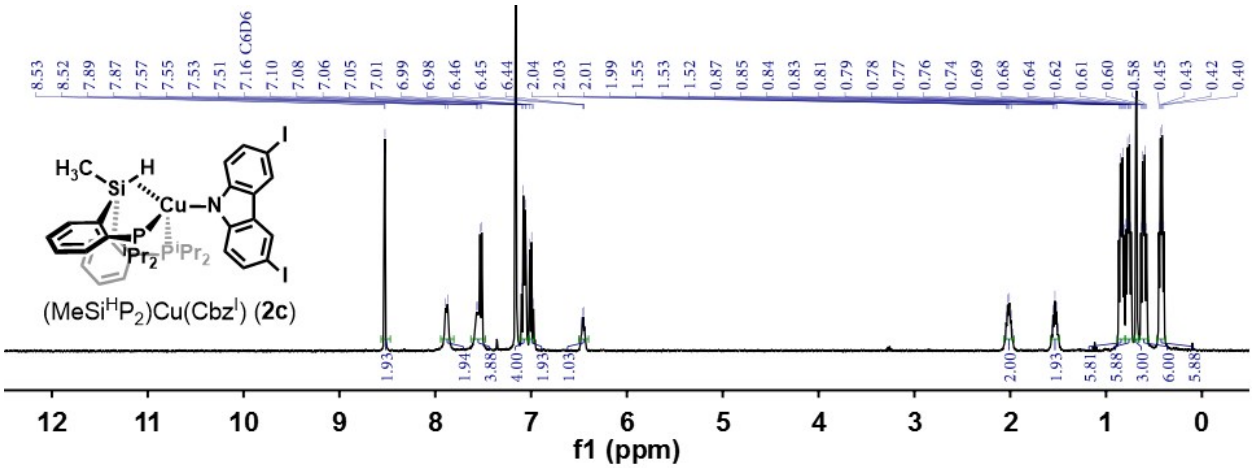

Figure S18. ^{13}C NMR spectrum (C_6D_6, 101 MHz) of (Si^HP_2)Cu(Cbz^I) (**2c**) at room temperature.

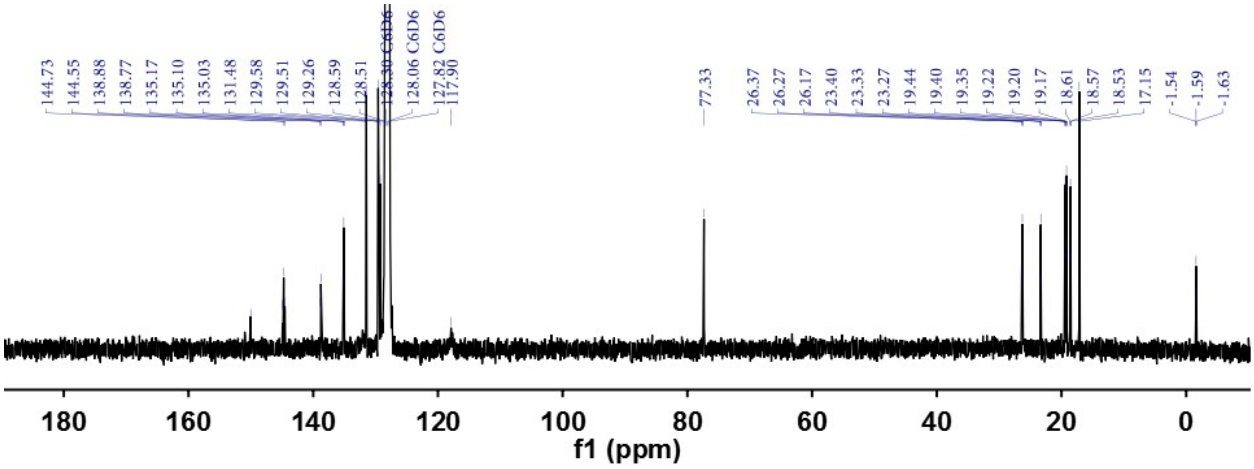

Figure S19. ^{29}Si NMR spectrum (THF/C_6D_6, 79 MHz) of (Si^HP_2)Cu(Cbz^I) (**2c**) in at room temperature.

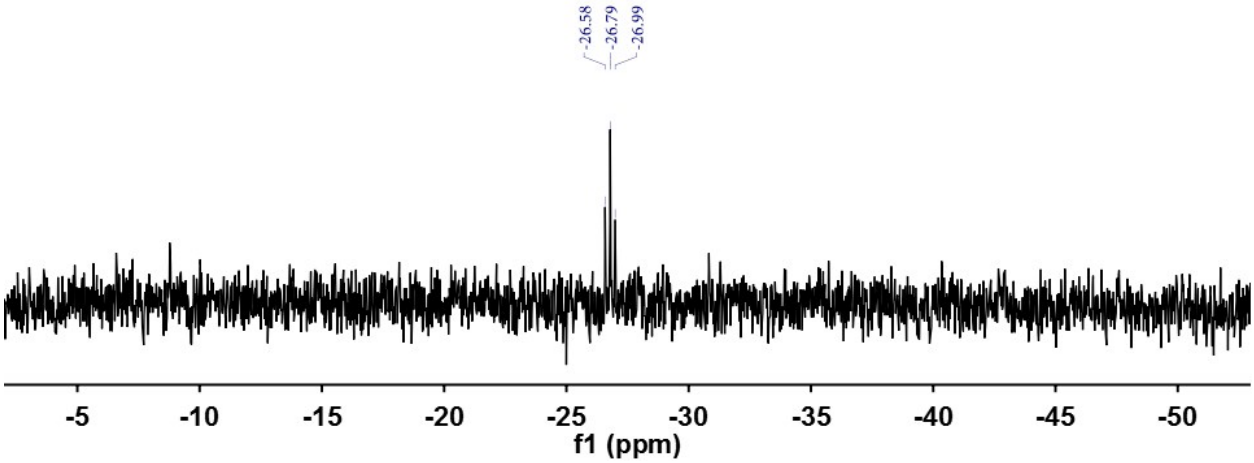

Figure S20. ^{31}P NMR spectrum (C_6D_6, 162 MHz) of (Si^HP_2)Cu(Cbz^I) (**2c**) at room temperature.

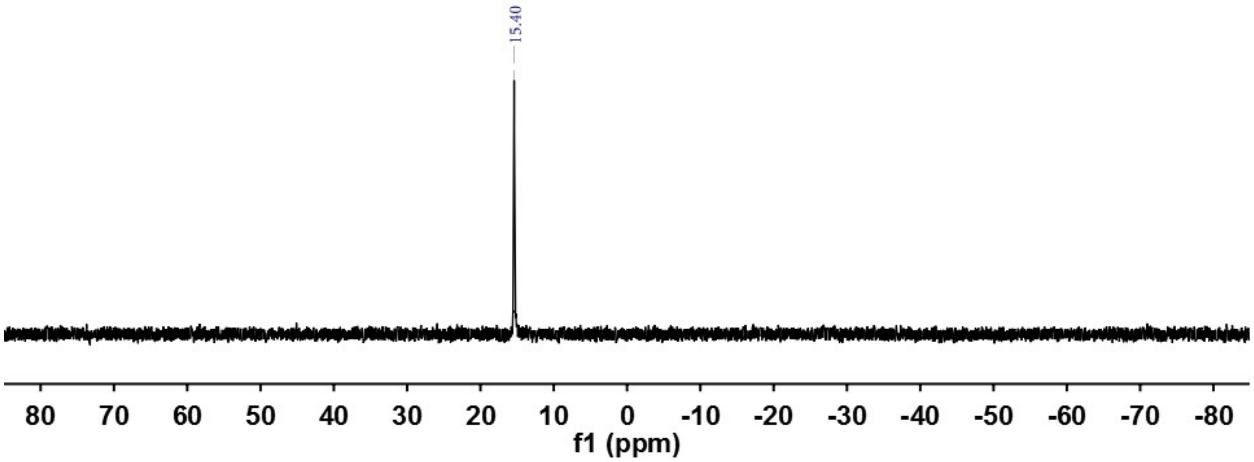

Figure S21. ^{1}H NMR spectrum (C_6D_6, 400 MHz) of ($PP^{Me}P$)CuCl (**3**) at room temperature.

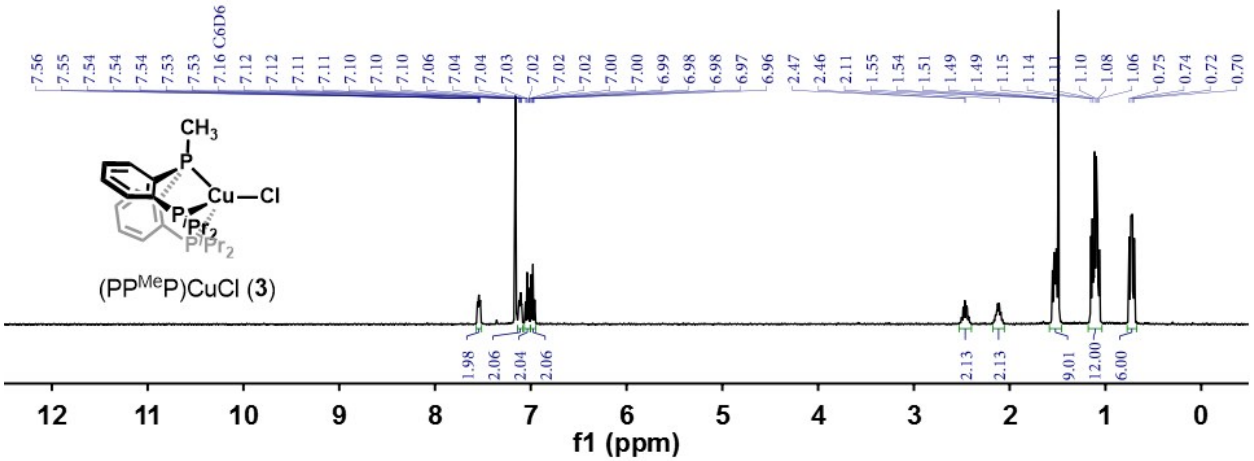

Figure S22. ^{13}C NMR spectrum (C_6D_6, 101 MHz) of ($PP^{Me}P$)CuCl (**3**) at room temperature.

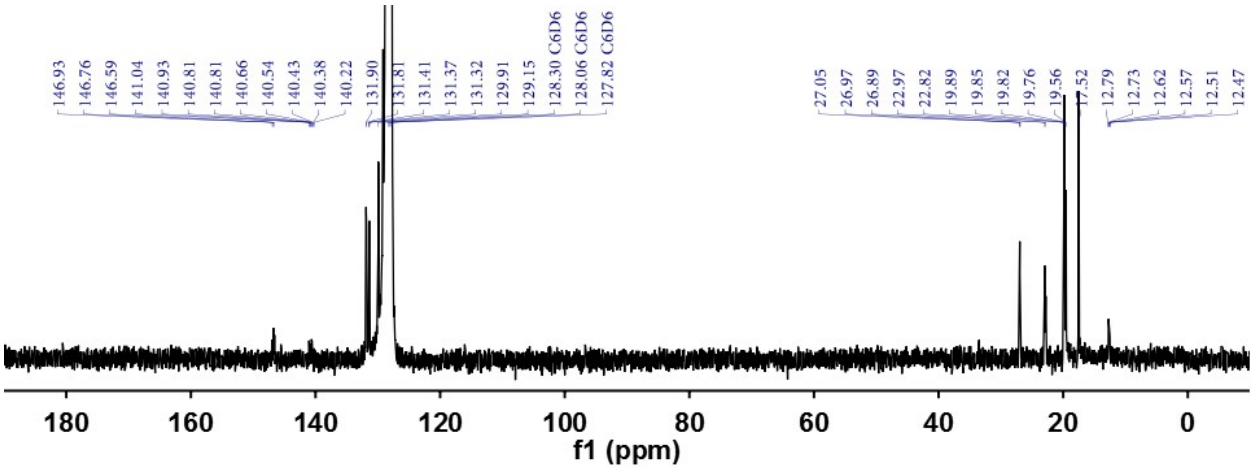

Figure S23. ^{31}P NMR spectrum (C_6D_6, 162 MHz) of ($PP^{Me}P$)CuCl (**3**) at room temperature.

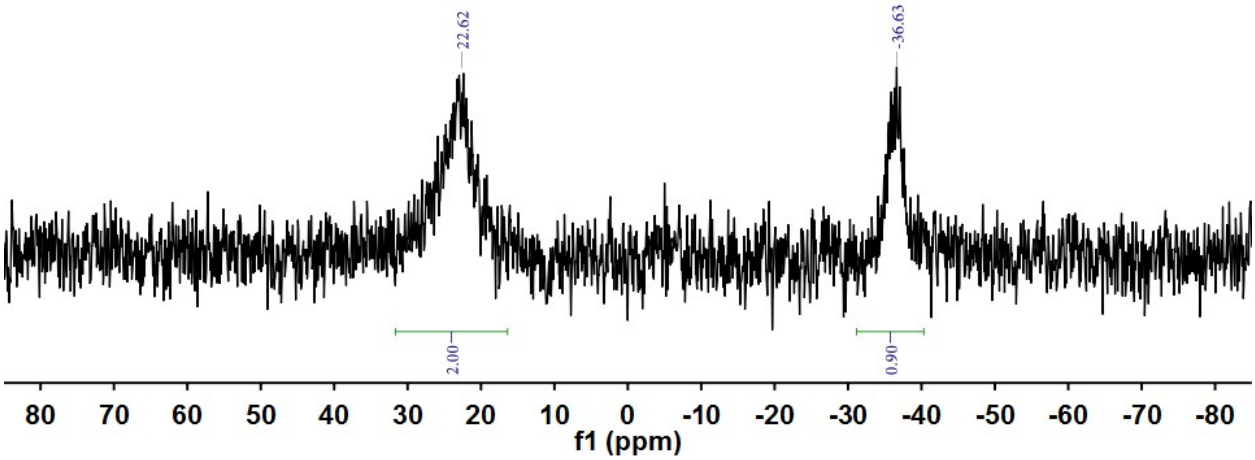

Figure S24. ^{1}H NMR spectrum (C_6D_6, 400 MHz) of ($PP^{Me}P$)Cu(Cbz) (**4a**) at room temperature.

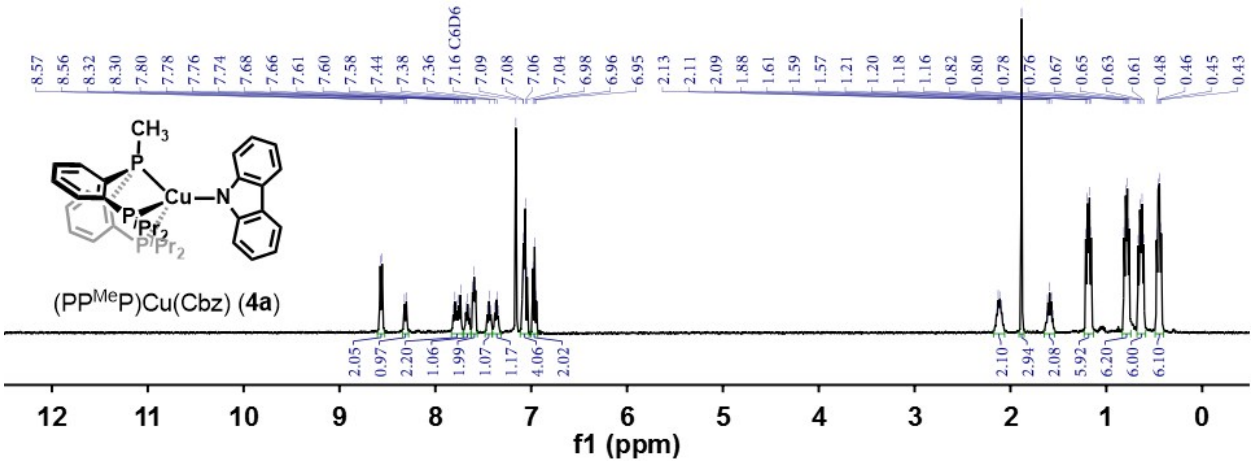

Figure S25. ^{13}C NMR spectrum (C_6D_6, 101 MHz) of ($PP^{Me}P$)Cu(Cbz) (**4a**) at room temperature.

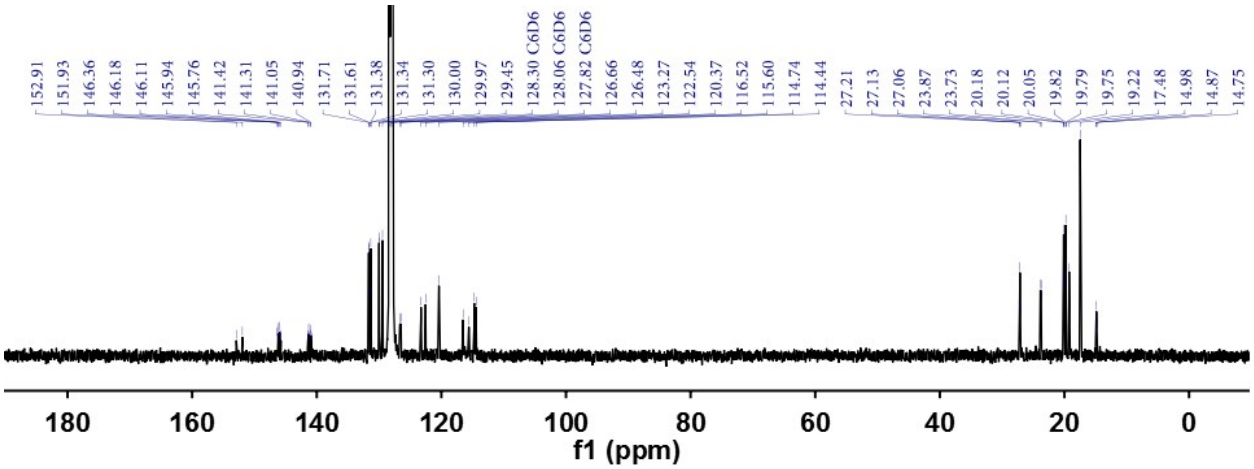

Figure S26. ^{31}P NMR spectrum (C_6D_6, 162 MHz) of ($PP^{Me}P$)Cu(Cbz) (**4a**) at room temperature.

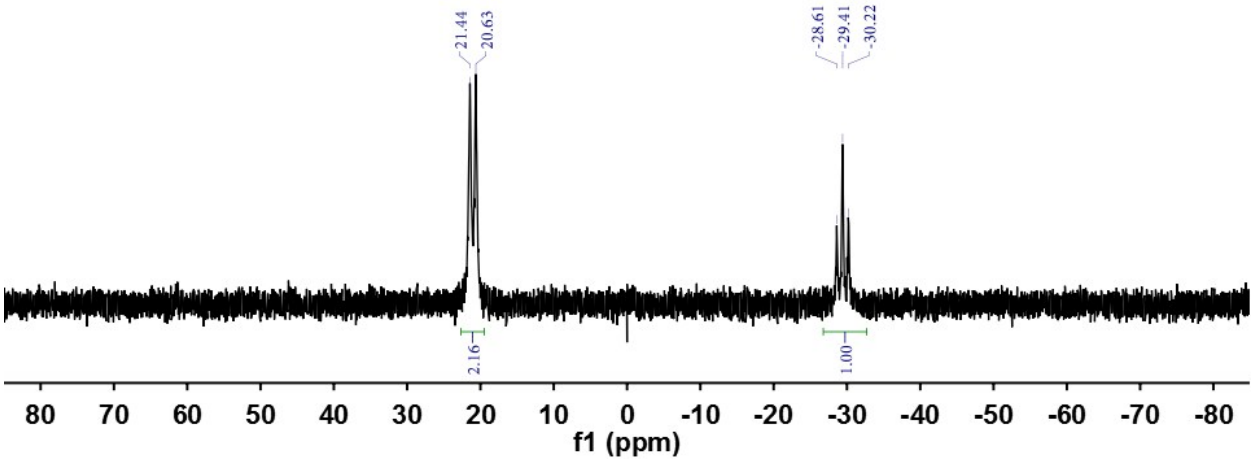

Figure S27. ^{1}H NMR spectrum (C_6D_6, 400 MHz) of ($PP^{Me}P$)Cu(Cbz^{t}Bu) (**4b**) at room temperature.

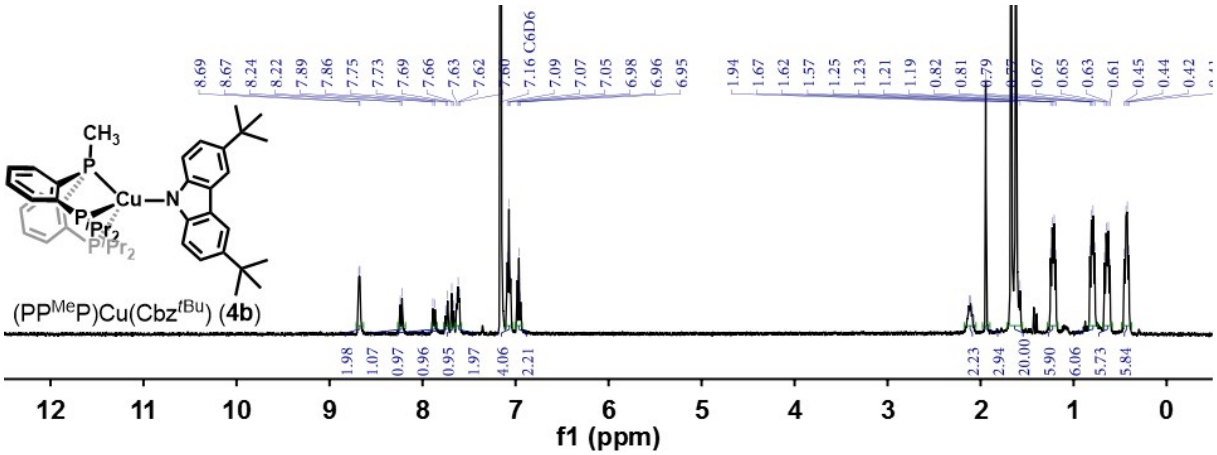

Figure S28. ^{13}C NMR spectrum (C_6D_6, 101 MHz) of ($PP^{Me}P$)Cu(Cbz^{t}Bu) (**4b**) at room temperature.

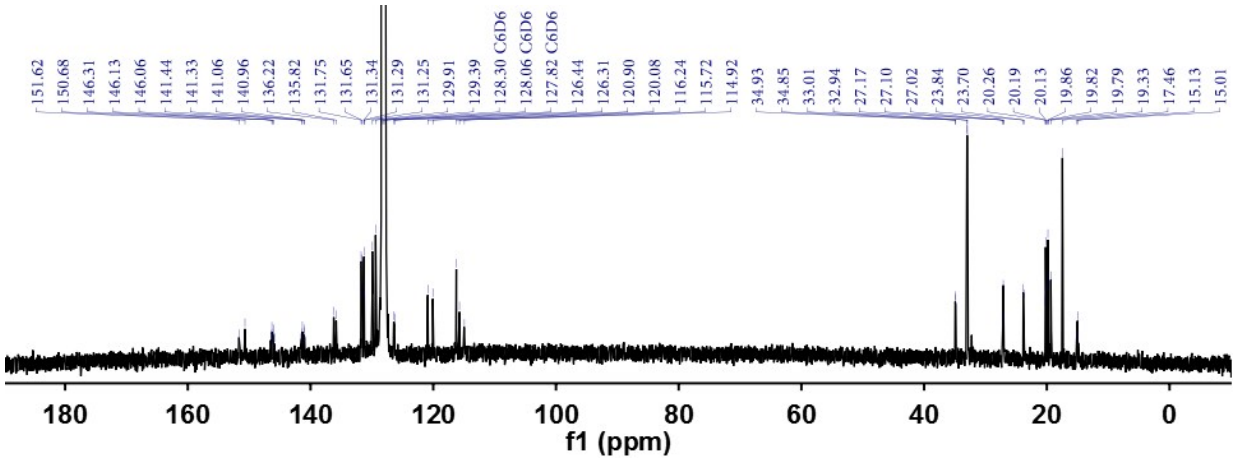

Figure S29. ^{31}P NMR spectrum (C_6D_6, 162 MHz) of ($PP^{Me}P$)Cu(Cbz^{t}Bu) (**4b**) at room temperature.

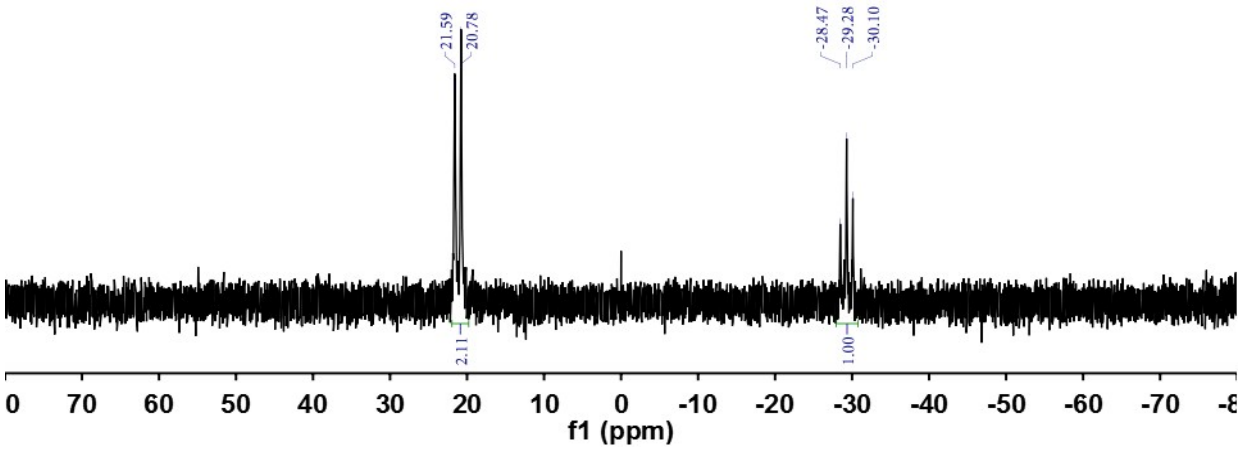

Figure S30. ^{1}H NMR spectrum (C_6D_6, 400 MHz) of ($PP^{Me}P$)Cu(Cbz^{I}) (**4c**) at room temperature.

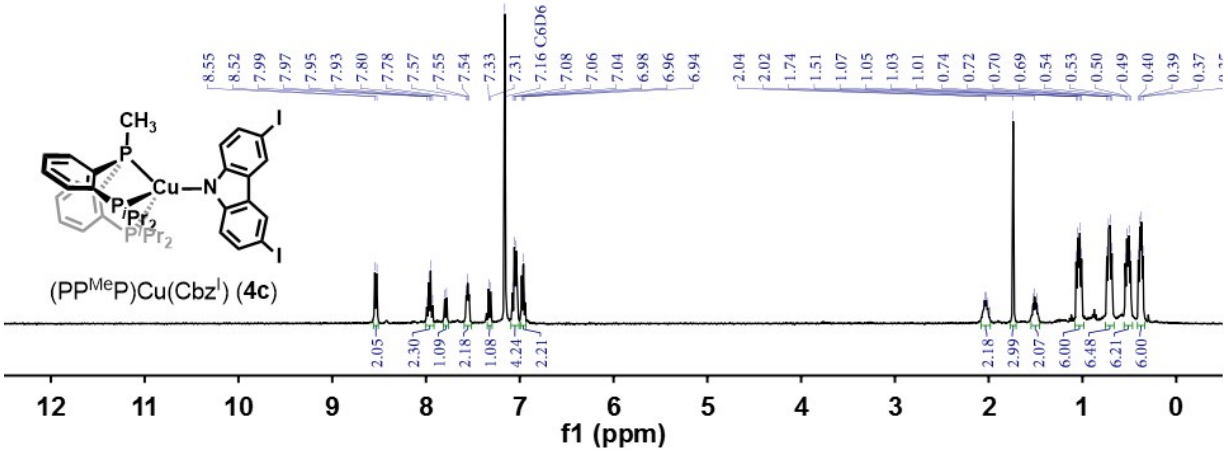

Figure S31. ^{13}C NMR spectrum (C_4D_8O, 101 MHz) of ($PP^{Me}P$)Cu(Cbz^I) (**4c**) at room temperature.

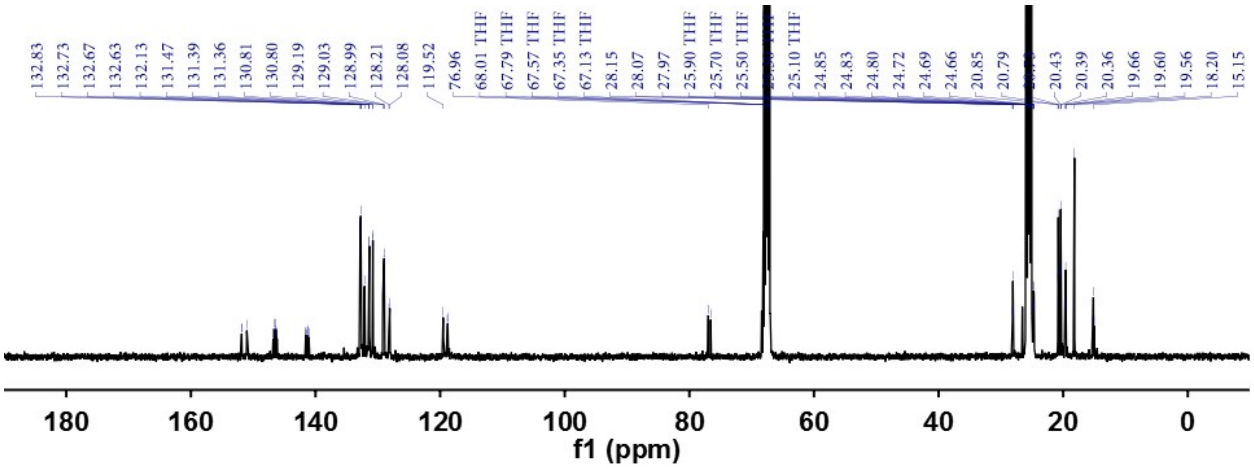

Figure S32. ^{31}P NMR spectrum (C_6D_6, 162 MHz) of ($PP^{Me}P$)Cu(Cbz^I) (**4c**) at room temperature.

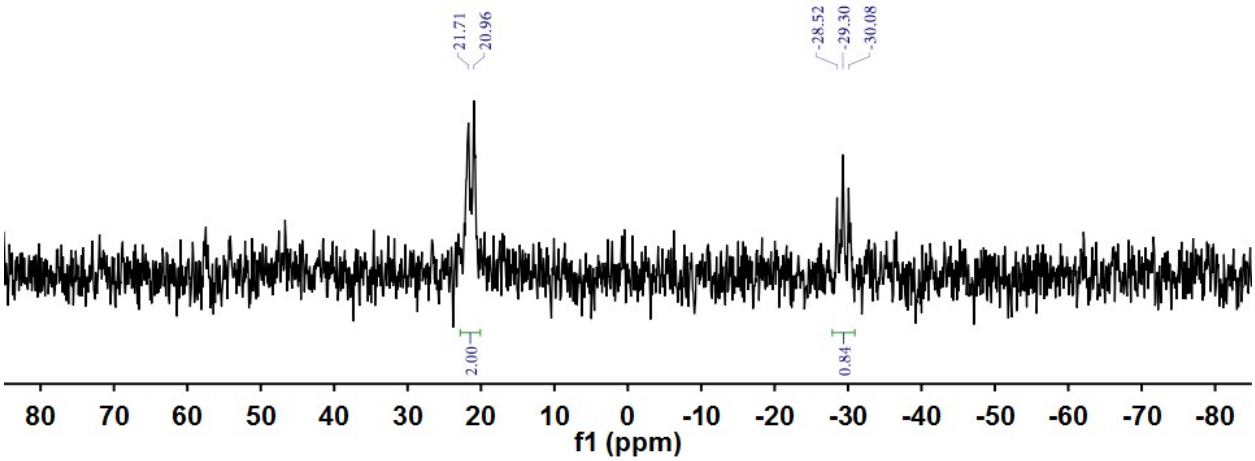

Figure S33. Solid state molecular structure of ($Si^{H}P_2$)CuCl (**1**). All hydrogen atoms except for the one bonded to Si atom are omitted for clarity. Si-H hydrogen was located on the Fourier difference map and its position was freely refined.

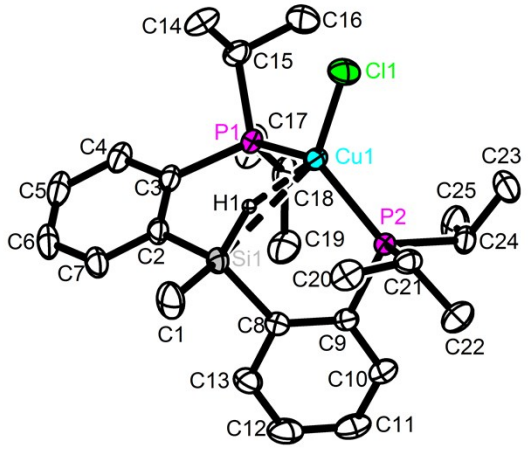

Table S1. Selected bond distances and angles for ($Si^{H}P_2$)CuCl (**1**) (Å and °).

Distance	**1**	Angle	**1**
$d_{Cu1-Si1}$	2.9163(4)	∠Si1–Cu1–Cl1	129.81(1)
d_{Cu1-P1}	2.2537(4)	∠Si1–Cu1–P1 ∠Si1–Cu1–P2	81.23(1) 81.75(1)
d_{Cu1-P2}	2.2624(4)	∠P1–Cu1–P2	127.12(1)
$d_{Cu1-Cl1}$	2.2680(4)	∠P1–Cu1–Cl1 ∠P2–Cu1–Cl1	118.28(1) 111.02(2)
d_{Cu1-H1}	1.98(2)		
d_{Si1-H1}	1.41(2)		

Figure S34. Solid state molecular structure of ($Si^{H}P_2$)Cu(Cbz) (**2a**). Co-crystallized solvent molecule and all hydrogen atoms except for the one bonded to Si atom are omitted for clarity. Si-H hydrogen was located on the Fourier difference map and its position was freely refined.

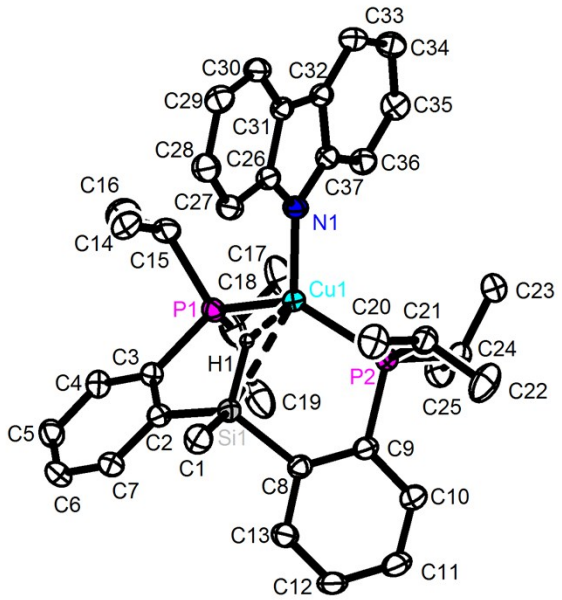

Table S2. Selected bond distances and angles for ($Si^{H}P_2$)Cu(Cbz) (**2a**) (Å and °).

Distance	**2a**	Angle	**2a**
$d_{Cu1-Si1}$	2.8485(6)	∠Si1–Cu1–N1	127.01(5)
d_{Cu1-P1}	2.2657(6)	∠Si1–Cu1–P1 ∠Si1–Cu1–P2	83.86(2) 84.10(2)
d_{Cu1-P2}	2.2620(5)	∠P1–Cu1–P2	132.06(2)
d_{Cu1-N1}	1.995(2)	∠P1–Cu1–N1 ∠P2–Cu1–N1	108.97(5) 115.24(5)
d_{Cu1-H1}	1.87(3)		
d_{Si1-H1}	1.46(3)		

Figure S35. Solid state molecular structure of $(Si^{H}P_2)Cu(Cbz^{tBu})$ (**2b**). All hydrogen atoms except for the one bonded to Si atom are omitted for clarity. Si-H hydrogen was located on the Fourier difference map and its position was freely refined.

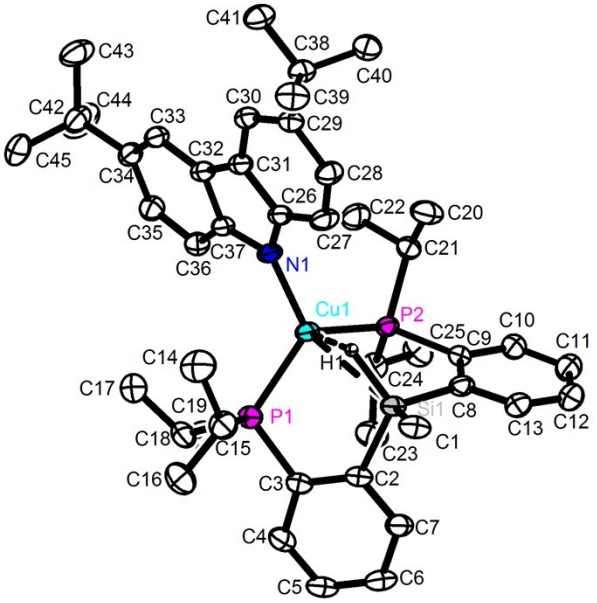

Table S3. Selected bond distances and angles for $(Si^{H}P_2)Cu(Cbz^{tBu})$ (**2b**) (Å and °).

Distance	**2b**	Angle	**2b**
$d_{Cu1-Si1}$	2.905(1)	∠Si1–Cu1–N1	131.1(1)
d_{Cu1-P1}	2.296(1)	∠Si1–Cu1–P1 ∠Si1–Cu1–P2	79.83(4) 80.82(4)
d_{Cu1-P2}	2.272(1)	∠P1–Cu1–P2	124.19(4)
d_{Cu1-N1}	1.984(3)	∠P1–Cu1–N1 ∠P2–Cu1–N1	117.0(1) 115.2(1)
d_{Cu1-H1}	1.86(6)		
d_{Si1-H1}	1.54(6)		

Figure S36. Solid state molecular structure of ($Si^{H}P_2$)Cu(Cbz^{I}) (**2c**). All hydrogen atoms except for the one bonded to Si atom are omitted for clarity. Si-H hydrogen was located on the Fourier difference map and its position was freely refined.

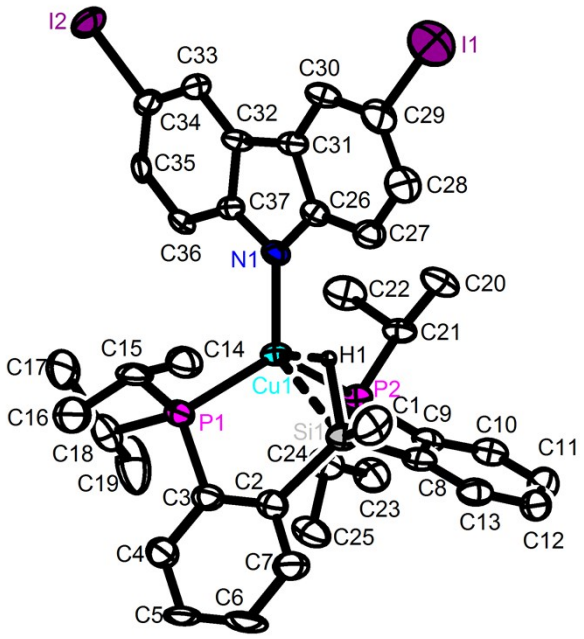

Table S4. Selected bond distances and angles for ($Si^{H}P_2$)Cu(Cbz^{I}) (**2c**) (Å and °).

Distance	**2c**	Angle	**2c**
$d_{Cu1-Si1}$	2.801(3)	∠Si1–Cu1–N1	119.4(2)
d_{Cu1-P1}	2.300(3)	∠Si1–Cu1–P1 ∠Si1–Cu1–P2	84.5(1) 82.9(1)
d_{Cu1-P2}	2.267(3)	∠P1–Cu1–P2	123.2(1)
d_{Cu1-N1}	1.986(8)	∠P1–Cu1–N1 ∠P2–Cu1–N1	117.7(3) 116.7(3)
d_{Cu1-H1}	1.8(1)		
d_{Si1-H1}	1.6(1)		

Figure S37. Solid state molecular structure of (PP^{Me}P)CuCl (**3**). All hydrogen atoms are omitted for clarity.

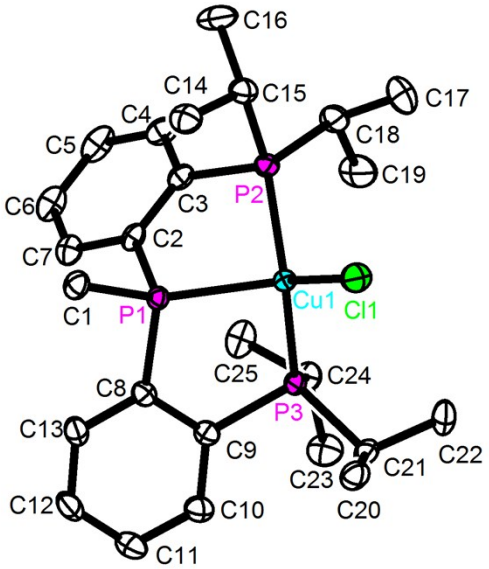

Table S5. Selected bond distances and angles for (PP^{Me}P)CuCl (**3**) (Å and °).

Distance	**3**	Angle	**3**
d_{Cu1-P1}	2.3085(8)	∠P1–Cu1–Cl1	125.78(3)
d_{Cu1-P2}	2.2647(8)	∠P1–Cu1–P2 ∠P1–Cu1–P3	88.43(3) 87.30(3)
d_{Cu1-P3}	2.2782(8)	∠P2–Cu1–P3	122.07(3)
$d_{Cu1-Cl1}$	2.2783(8)	∠P2–Cu1–Cl1 ∠P3–Cu1–Cl1	111.88(3) 116.96(3)

Figure S38. Solid state molecular structure of (PP^{Me}P)Cu(Cbz) (**4a**). Co-crystallized solvent molecule and all hydrogen atoms are omitted for clarity.

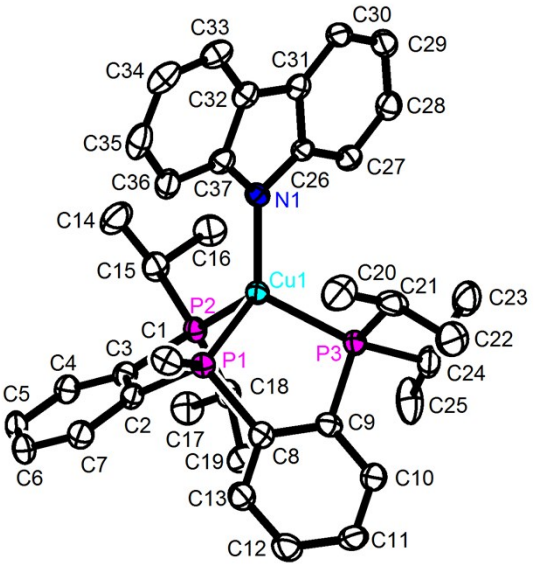

Table S6. Selected bond distances and angles for (PP^{Me}P)Cu(Cbz) (**4a**) (Å and °).

Distance	**4a**	Angle	**4a**
d_{Cu1-P1}	2.2802(8)	∠P1–Cu1–N1	122.26(7)
d_{Cu1-P2}	2.2571(9)	∠P1–Cu1–P2 ∠P1–Cu1–P3	88.35(3) 88.53(3)
d_{Cu1-P3}	2.2905(8)	∠P2–Cu1–P3	121.72(3)
d_{Cu1-N1}	1.993(2)	∠P2–Cu1–N1 ∠P3–Cu1–N1	117.23(8) 113.14(8)

Figure S39. Solid state molecular structure of (PP^{Me}P)Cu(Cbz^{tBu}) (**4b**). All hydrogen atoms are omitted for clarity.

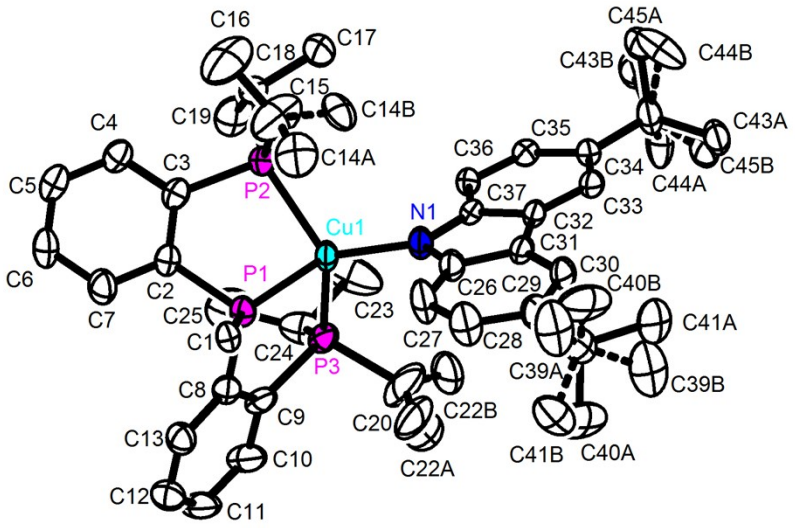

Table S7. Selected bond distances and angles for (PP^{Me}P)Cu(Cbz^{tBu}) (**4b**) (Å and °).

Distance	**4b**	Angle	**4b**
$d_{Cu1–P1}$	2.266(1)	∠P1–Cu1–N1	127.59(9)
$d_{Cu1–P2}$	2.283(1)	∠P1–Cu1–P2 ∠P1–Cu1–P3	87.78(4) 88.11(4)
$d_{Cu1–P3}$	2.274(1)	∠P2–Cu1–P3	128.31(4)
$d_{Cu1–N1}$	1.980(3)	∠P2–Cu1–N1 ∠P3–Cu1–N1	113.5(1) 109.4(1)

Figure S40. Solid state molecular structure of ($PP^{Me}P$)Cu(Cbz^{I}) (**4c**). All hydrogen atoms are omitted for clarity.

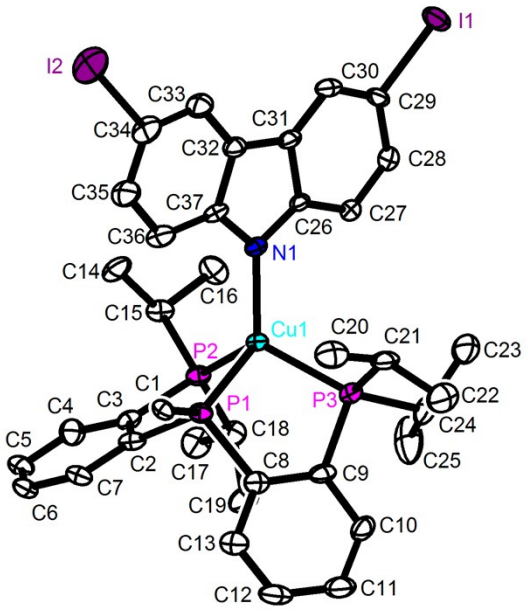

Table S8. Selected bond distances and angles for ($PP^{Me}P$)Cu(Cbz^{I}) (**4c**) (Å and °).

Distance	**4c**	Angle	**4c**
$d_{Cu1–P1}$	2.275(2)	∠P1–Cu1–N1	122.2(2)
$d_{Cu1–P2}$	2.264(2)	∠P1–Cu1–P2 ∠P1–Cu1–P3	87.84(7) 88.95(6)
$d_{Cu1–P3}$	2.290(2)	∠P2–Cu1–P3	121.32(6)
$d_{Cu1–N1}$	1.992(5)	∠P2–Cu1–N1 ∠P3–Cu1–N1	115.7(2) 115.1(2)

Figure S41. Overlay of the core structures of ($Si^{H}P_2$)Cu(Cbz) (**2a**) (red) and ($Si^{H}P_2$)Cu(Cbz^{tBu}) (**2b**) (blue): (a) top-view and (b) side-view.

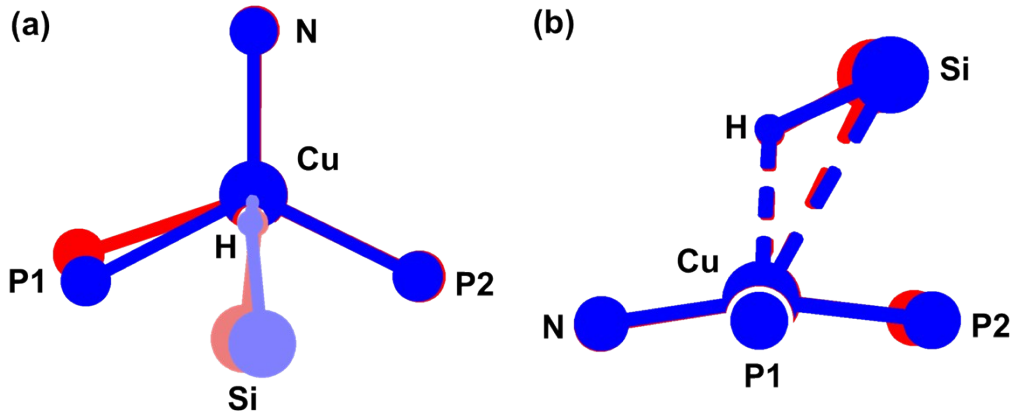

Figure S42. UV-Vis spectra of ($Si^{H}P_2$)CuCl (**1**) (dotted green), carbazole (dotted black) and ($Si^{H}P_2$)Cu(Cbz) (**2a**) (red) in THF at room temperature.

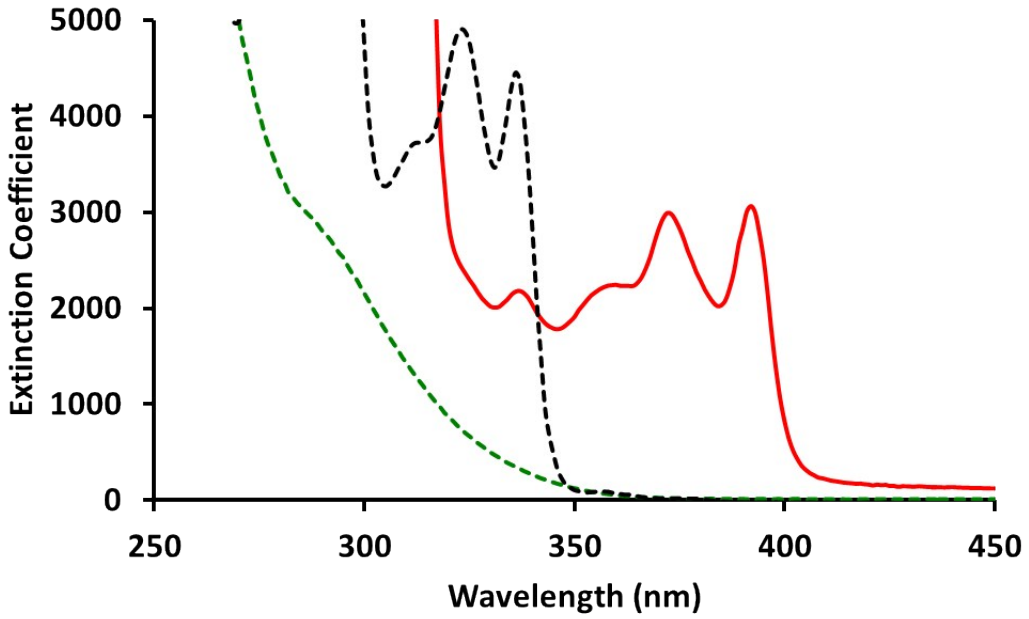

Figure S43. UV-Vis spectra of ($Si^{H}P_2$)Cu(Cbz) (**2a**) (blue), ($Si^{H}P_2$)Cu(Cbz^{tBu}) (**2b**) (green) and ($Si^{H}P_2$)Cu(Cbz^{I}) (**2c**) (red) in THF at room temperature.

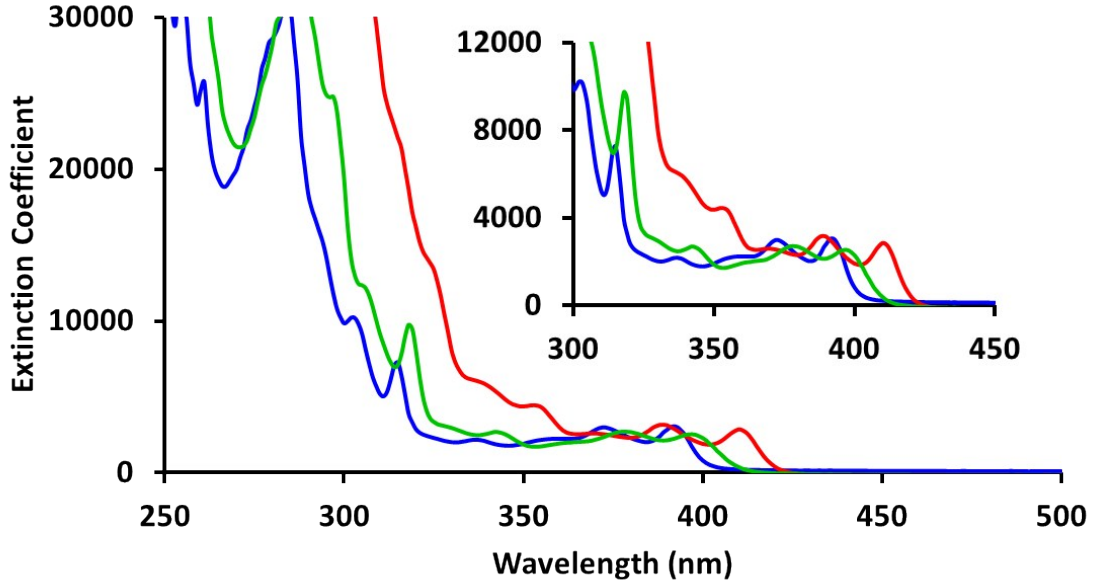

Figure S44. UV-Vis spectra of ($PP^{Me}P$)Cu(Cbz) (**4a**) (blue), ($PP^{Me}P$)Cu(Cbz^{tBu}) (**4b**) (green) and ($PP^{Me}P$)Cu(Cbz^{I}) (**4c**) (red) in THF at room temperature.

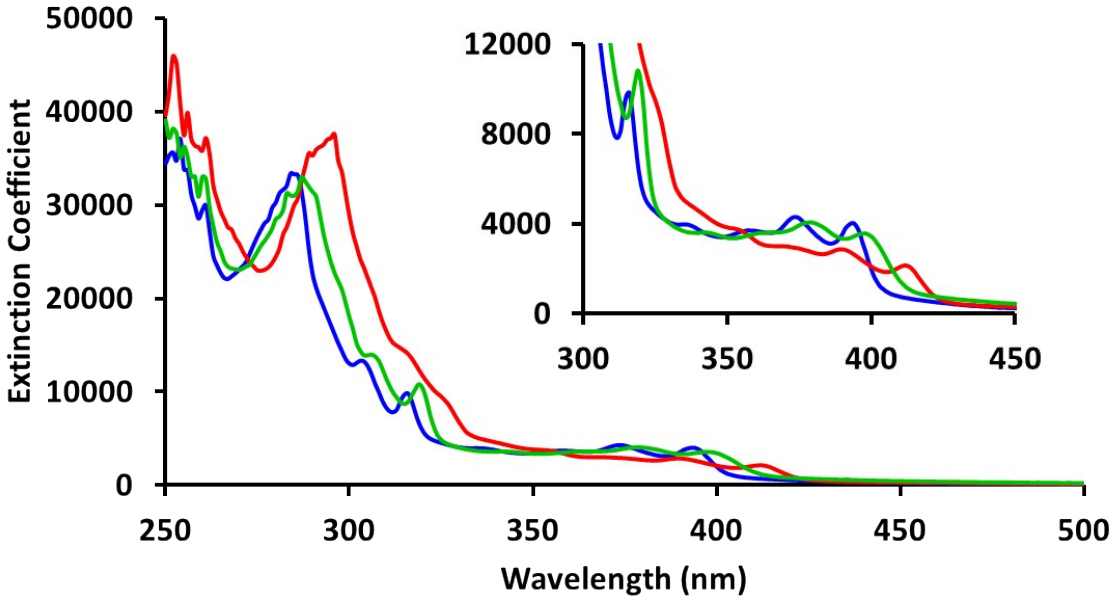

Figure S45. UV-Vis spectra of ($Si^{H}P_2$)Cu(Cbz) (**2a**) (red) and ($PP^{Me}P$)Cu(Cbz) (**4a**) (blue) in THF at room temperature.

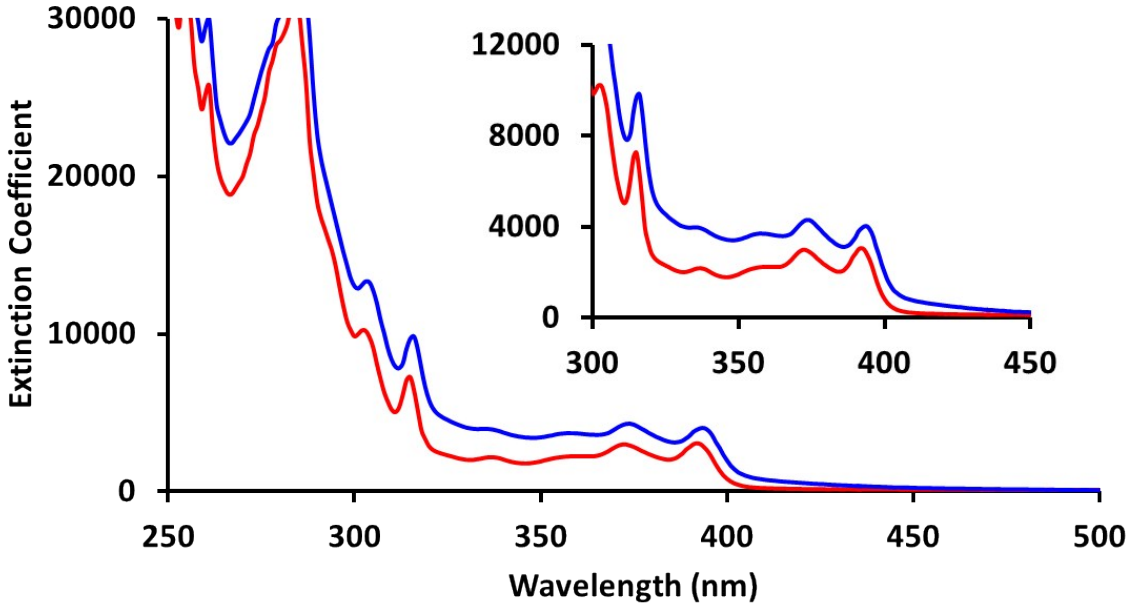

Figure S46. Emission spectra of ($Si^{H}P_2$)Cu(Cbz) (**2a**) with λ_{ex} = 392 nm (red), λ_{ex} = 372 nm (blue) and λ_{ex} = 314 nm (black) in THF at room temperature.

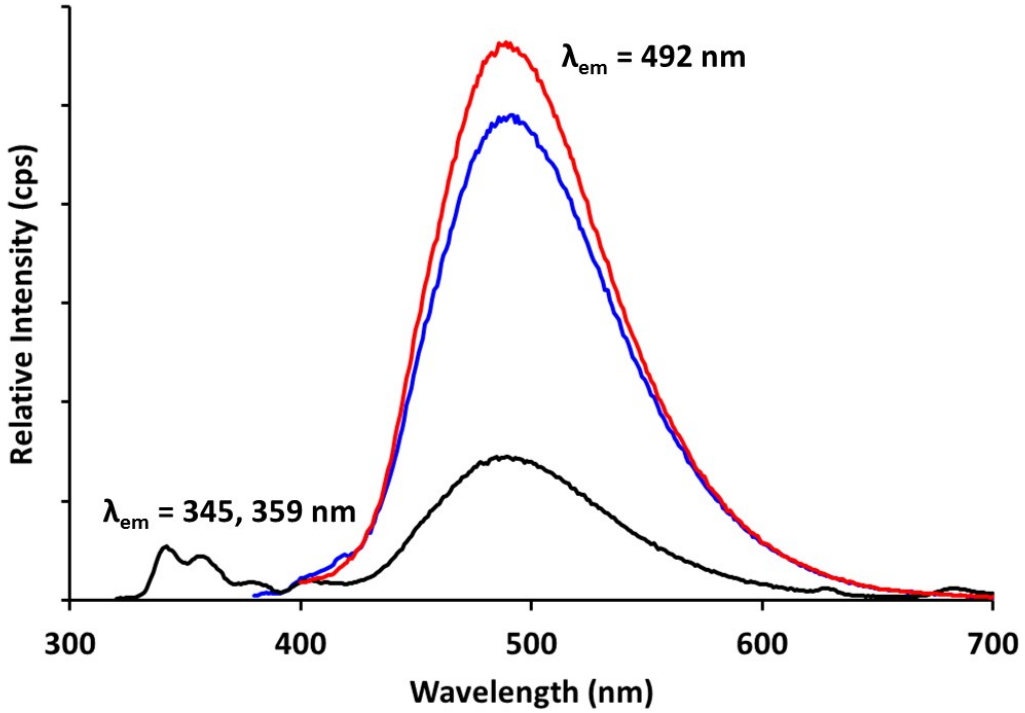

Figure S47. Emission spectra of ($Si^{H}P_2$)Cu(Cbz) (**2a**) with λ_{ex} = 392 nm (red), λ_{ex} = 372 nm (blue) and λ_{ex} = 314 nm (black) in toluene at room temperature.

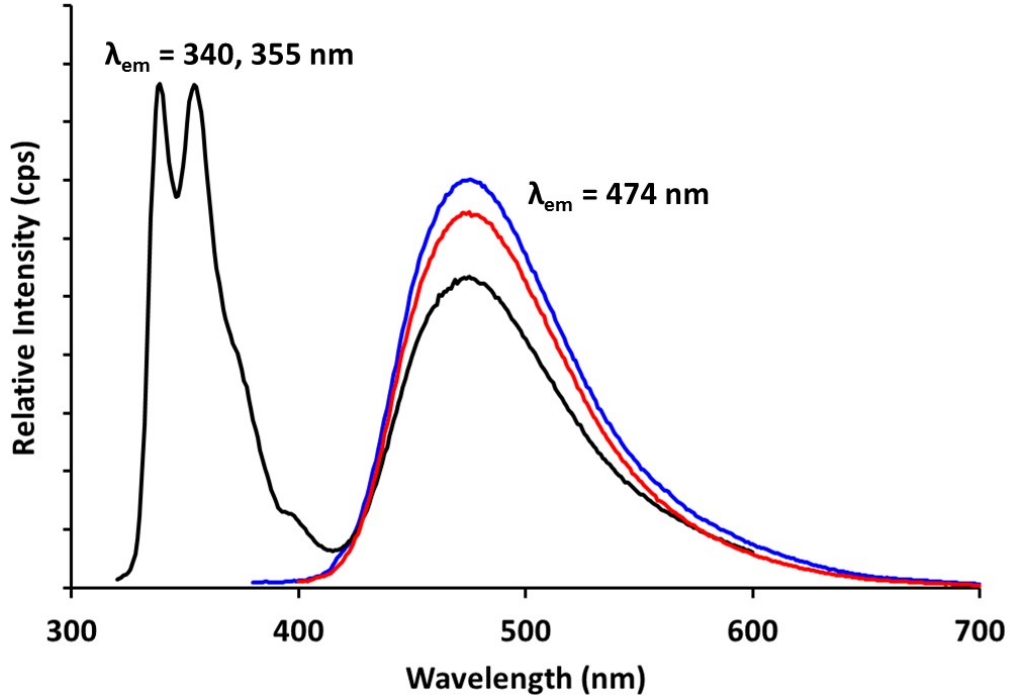

Figure S48. Emission spectra of ($Si^{H}P_2$)Cu(Cbz) (**2a**) with λ_{ex} = 392 nm (red), λ_{ex} = 372 nm (blue) and λ_{ex} = 314 nm (black) in benzene at room temperature.

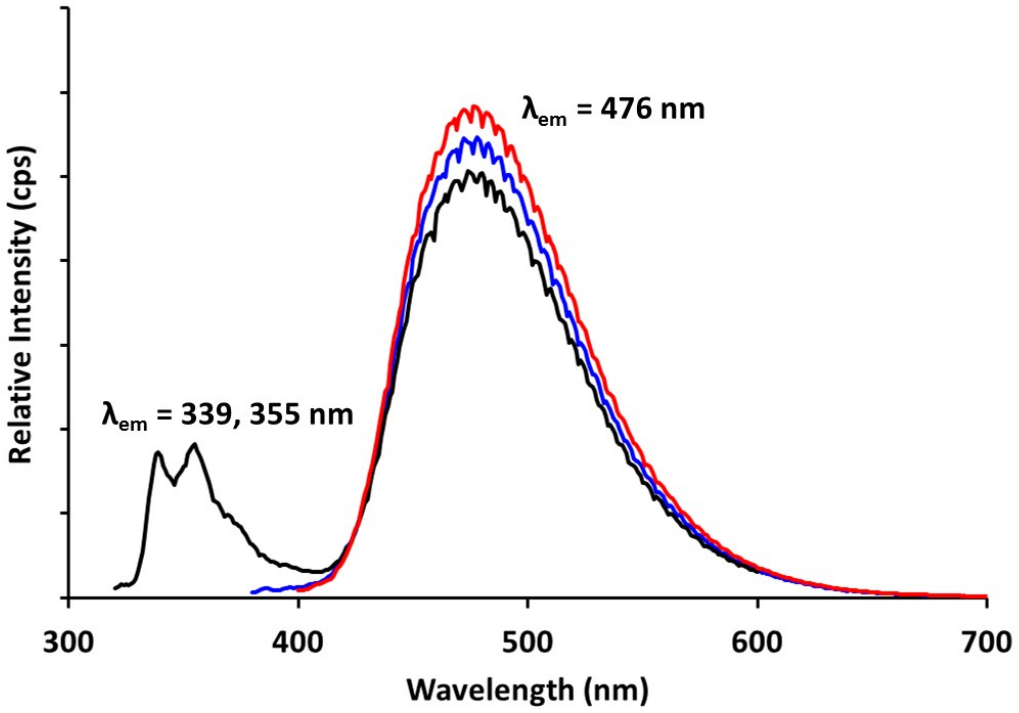

Figure S49. Emission spectra of ($Si^{H}P_2$)Cu(Cbz) (**2a**) with λ_{ex} = 392 nm (red), λ_{ex} = 372 nm (blue) and λ_{ex} = 314 nm (black) in acetonitrile at room temperature.

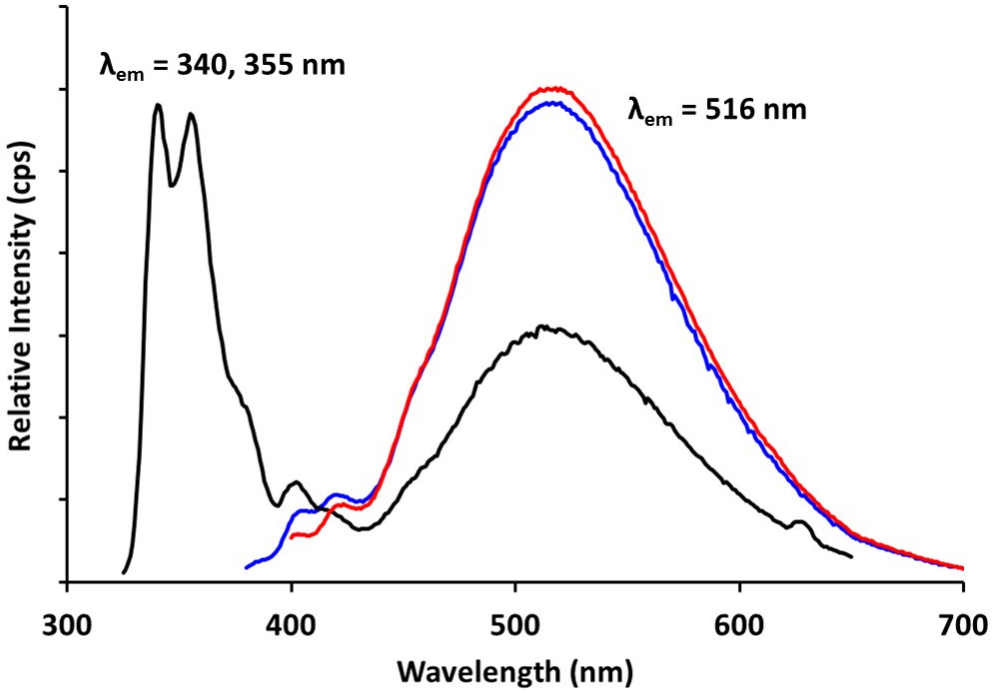

Figure S50. Emission spectra of ($Si^{H}P_2$)Cu(Cbz^{tBu}) (**2b**) with λ_{ex} = 397 nm (red), λ_{ex} = 378 nm (blue) and λ_{ex} = 318 nm (black) in THF at room temperature.

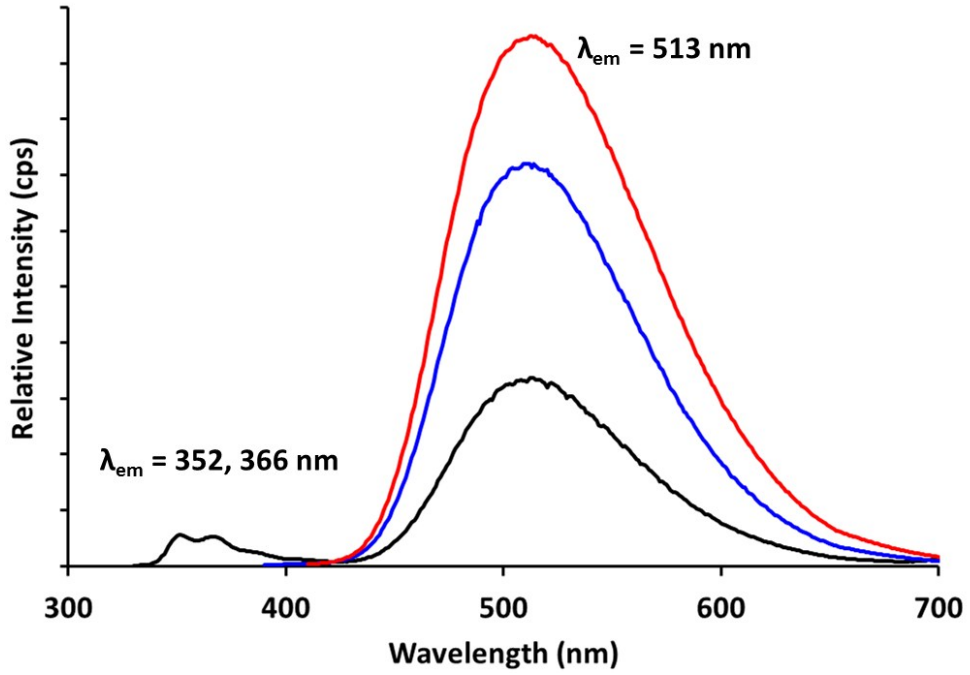

Figure S51. Emission spectra of ($Si^{H}P_2$)Cu(Cbz^{I}) (**2c**) with λ_{ex} = 410 nm (red), λ_{ex} = 389 nm (blue) and λ_{ex} = 325 nm (black) in THF at room temperature. The inset shows background emission spectra of THF at room temperature with λ_{ex} = 410 nm (red) and λ_{ex} = 389 nm (blue).

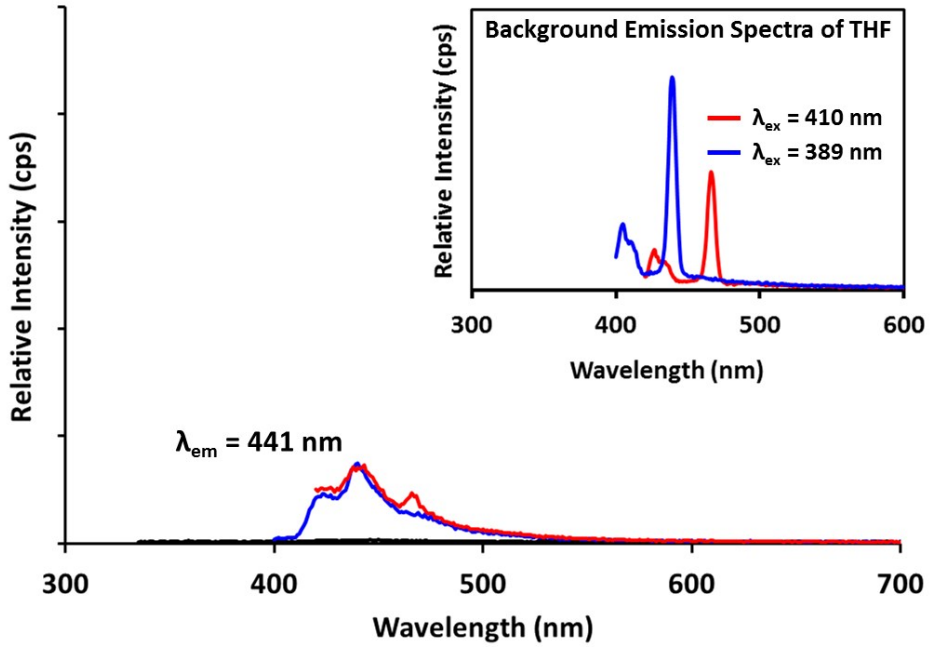

Figure S52. Excitation (dotted) and emission (solid) spectra of ($Si^{H}P_2$)Cu(Cbz) (**2a**, λ_{ex} = 392 nm, λ_{em} = 492 nm) (red), ($Si^{H}P_2$)Cu(Cbz^{tBu}) (**2b**, λ_{ex} = 397 nm, λ_{em} = 513 nm) (blue) and ($Si^{H}P_2$)Cu(Cbz^{I}) (**2c**, λ_{ex} = 398 nm, λ_{em} = 441 nm) (green) in THF at room temperature.

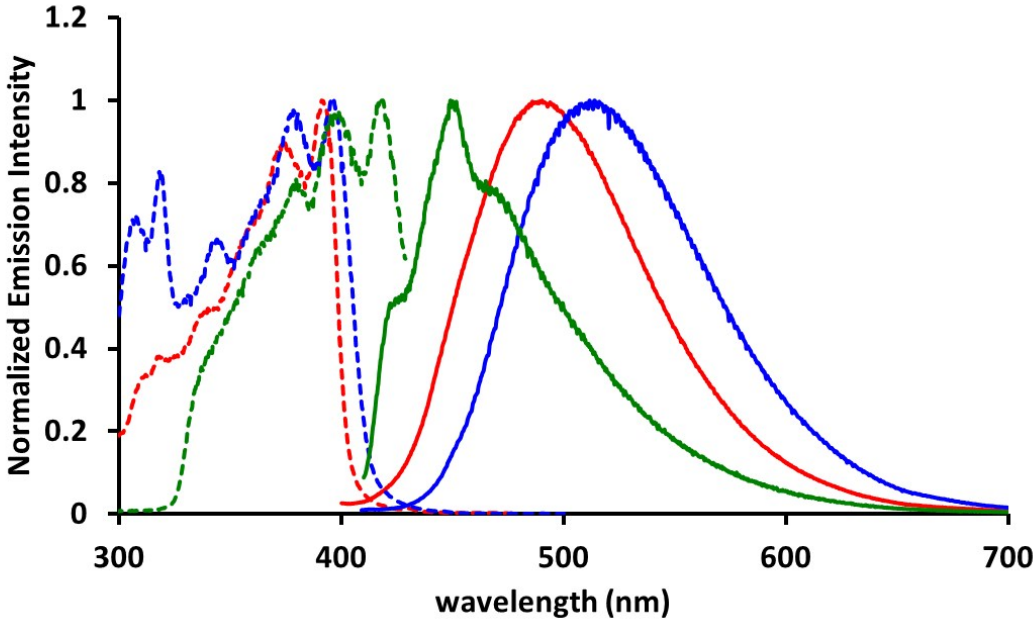

Figure S53. Excitation (dotted) and emission (solid) spectra of ($Si^{H}P_2$)Cu(Cbz) (**2a**, λ_{ex} = 392 nm, λ_{em} = 474 nm) (red) and ($Si^{H}P_2$)Cu(Cbz^{tBu}) (**2b**, λ_{ex} = 397 nm, λ_{em} = 490 nm) (blue) in toluene at room temperature.

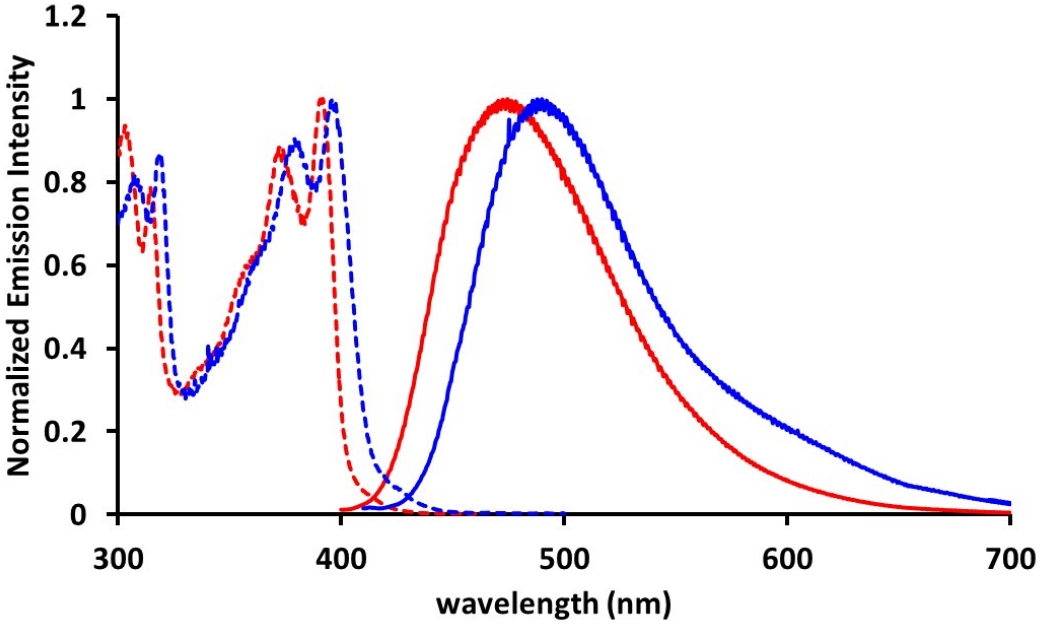

Figure S54. Emission spectra of (PP^{Me}P)Cu(Cbz) (**4a**) with λ_{ex} = 392 nm (red), λ_{ex} = 372 nm (blue) and λ_{ex} = 313 nm (black) in THF at room temperature. The inset shows background emission spectra of THF at room temperature with λ_{ex} = 392 nm (red) and λ_{ex} = 372 nm (blue).

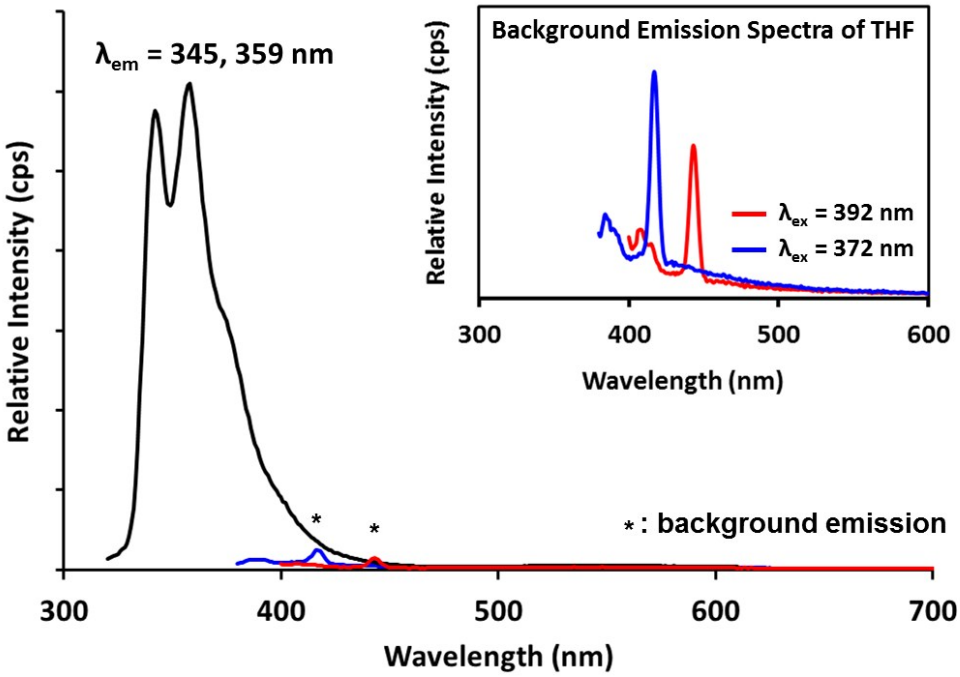

Figure S55. Emission spectra of (PP^{Me}P)Cu(Cbz^{tBu}) (**4b**) with λ_{ex} = 398 nm (red), λ_{ex} = 379 nm (blue) and λ_{ex} = 319 nm (black) in THF at room temperature. The inset shows background emission spectra of THF at room temperature with λ_{ex} = 398 nm (red) and λ_{ex} = 379 nm (blue).

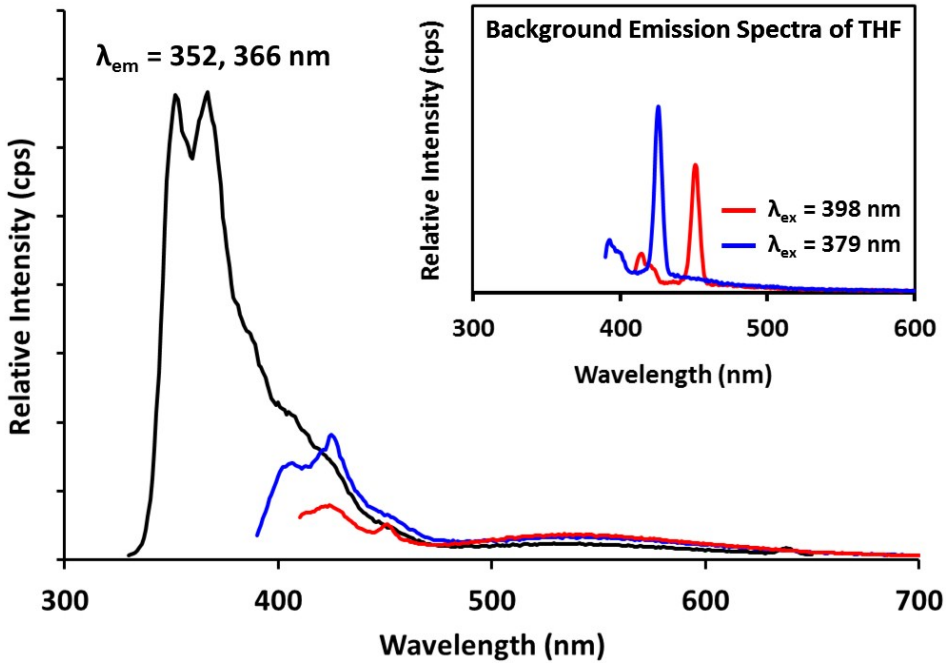

Figure S56. Emission spectra of ($PP^{Me}P$)Cu(Cbz^{I}) (**4c**) with λ_{ex} = 408 nm (red), λ_{ex} = 390 nm (blue) and λ_{ex} = 315 nm (black) in THF at room temperature. The inset shows background emission spectra of THF at room temperature with λ_{ex} = 408 nm (red) and λ_{ex} = 390 nm (blue).

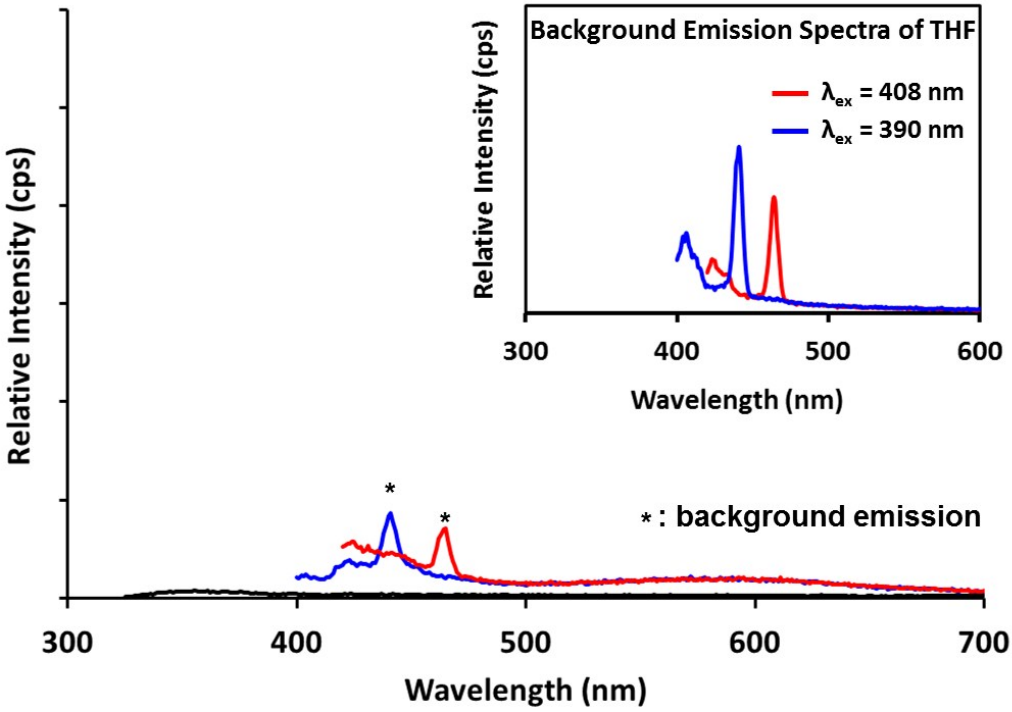

Figure S57. Emission spectrum of carbazole in THF at room temperature.

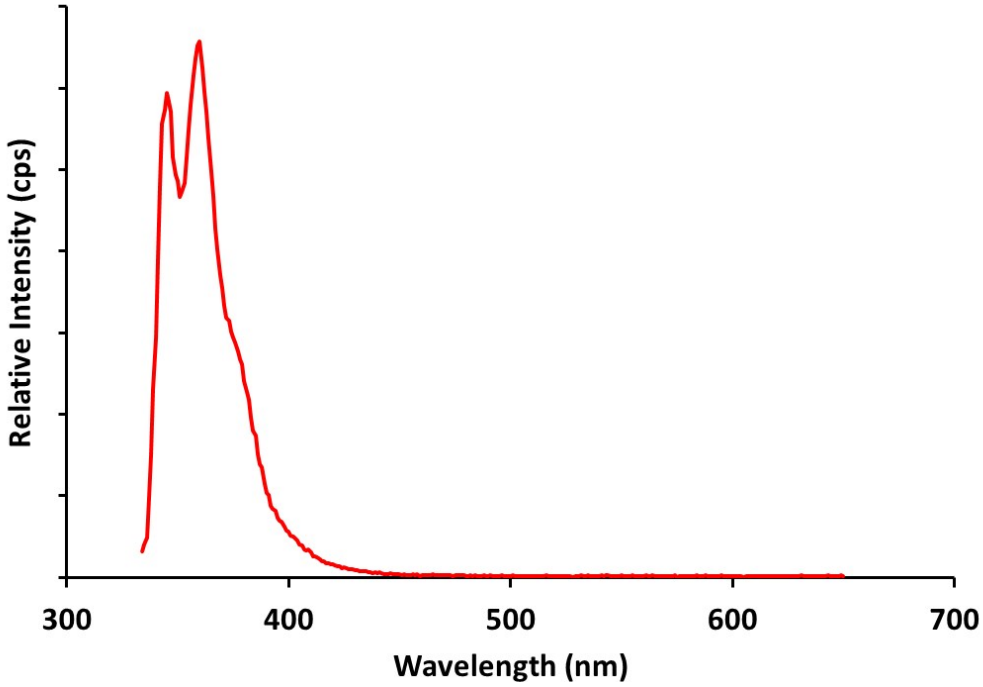

Figure S58. (a) Absorption of ($Si^{H}P_2$)Cu(Cbz) (**2a**) (red), ($PP^{Me}P$)Cu(Cbz) (**4a**) (blue), and carbazole (black) and (b) their emission spectra; the emission spectra were obtained with excitation at λ_{ex} = 372 nm (solid) and 314 nm (dashed) for **2a** and **4a** and λ_{ex} = 324 nm for carbazole.

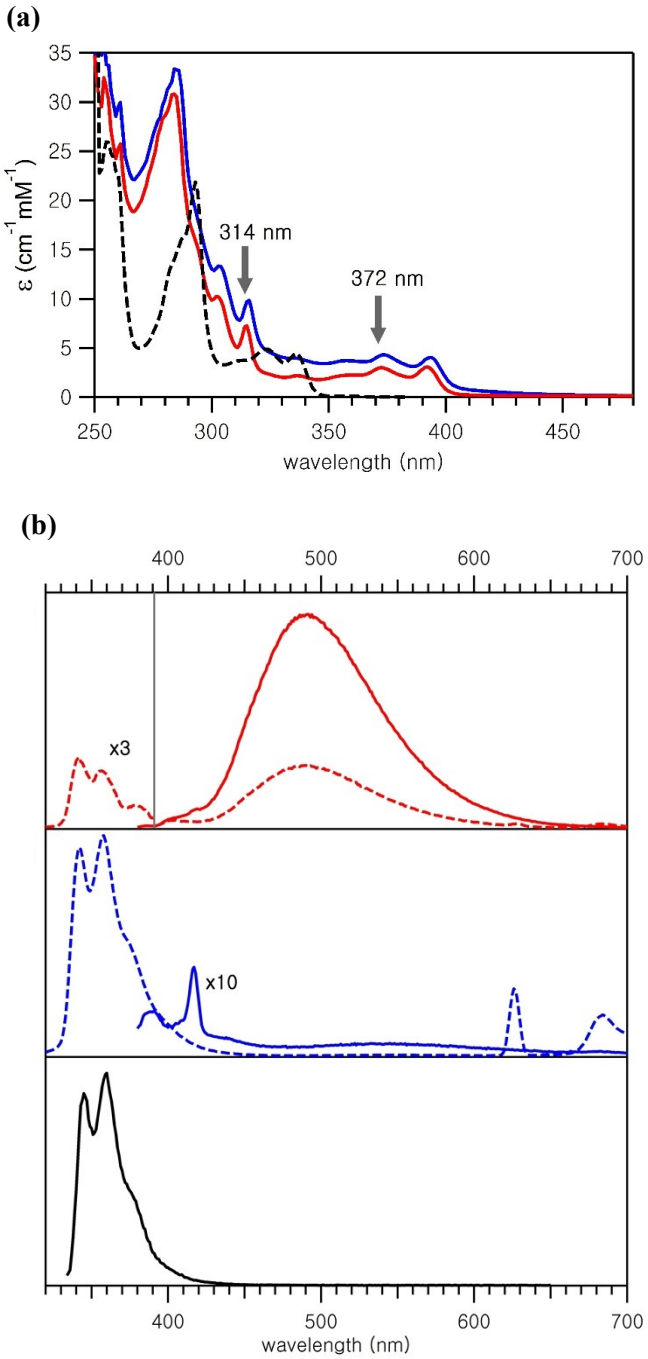

Figure S59. (a) Emission spectra of ($Si^{H}P_2$)Cu(Cbz) (**2a**, λ_{ex} = 392 nm) in THF at various temperatures and (b) plot of 1/T vs ln(F(S1)); F(S1) = integrated intensity, T = 220 K to 300 K.

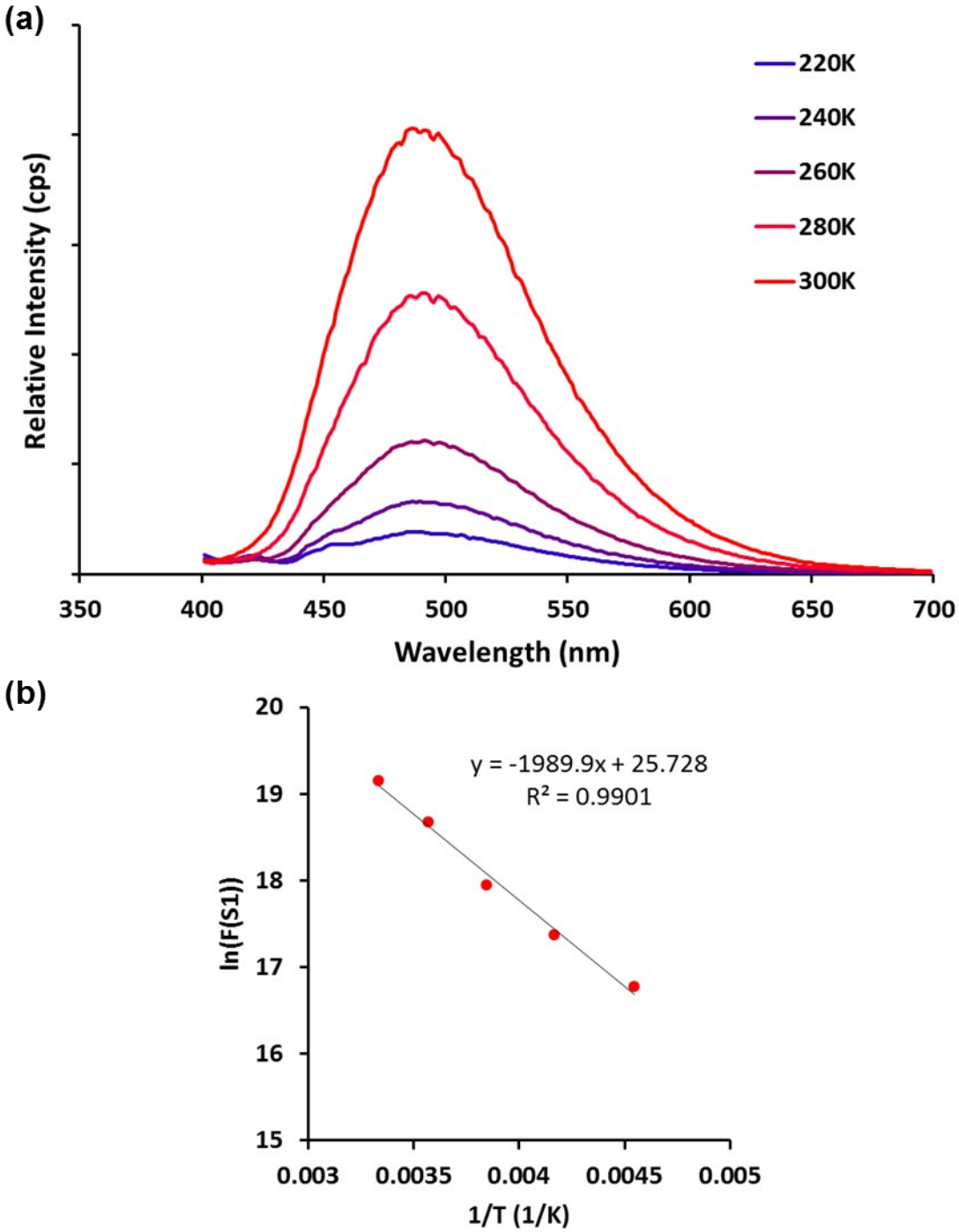

$$\ln F(T_1) - \ln F(S_1) = \frac{\Delta E_{ST}1}{k \quad T}$$

From the equation, ΔE_{ST} = 1989.9 K × (8.6173324 × 10^{-5} eV K^{-1}) = ~ 0.17148 eV.

Figure S60. (a) Emission spectra of ($Si^{H}P_2$)Cu(Cbz^{tBu}) (**2b**, λ_{ex} = 397 nm) in THF at various temperatures and (b) plot of 1/T vs ln(F(S1)); F(S1) = integrated intensity, T = 220 K to 300 K.

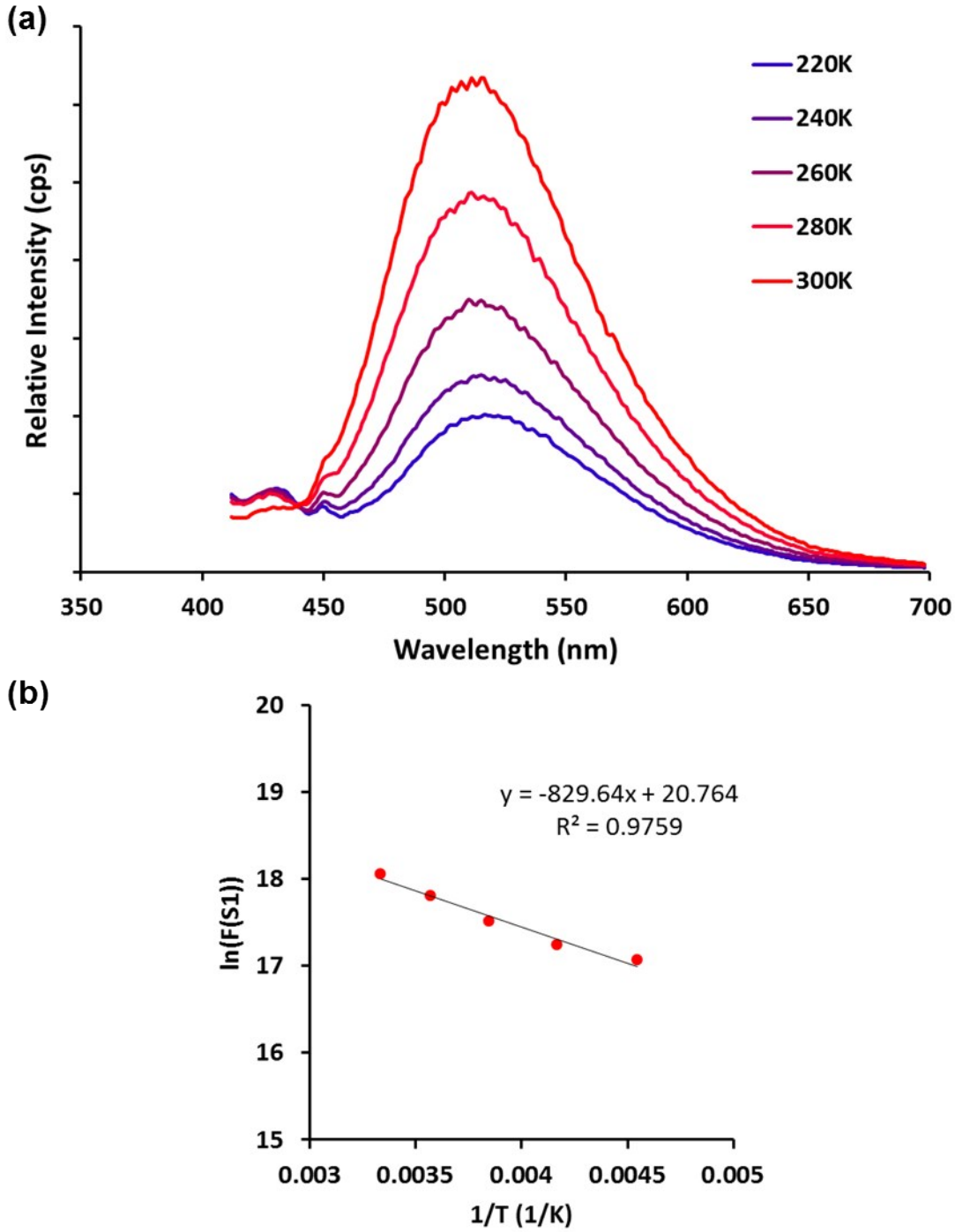

$$\ln F(T_1) - \ln F(S_1) = \frac{\Delta E_{ST}1}{k \quad T}$$

From the equation, ΔE_{ST} = 829.64 K × (8.6173324 × 10^{-5} eV K^{-1}) = ~ 0.071493 eV.

Figure S61. Luminescence decay trace of ($Si^{H}P_2$)Cu(Cbz) (**2a**) in THF at room temperature.

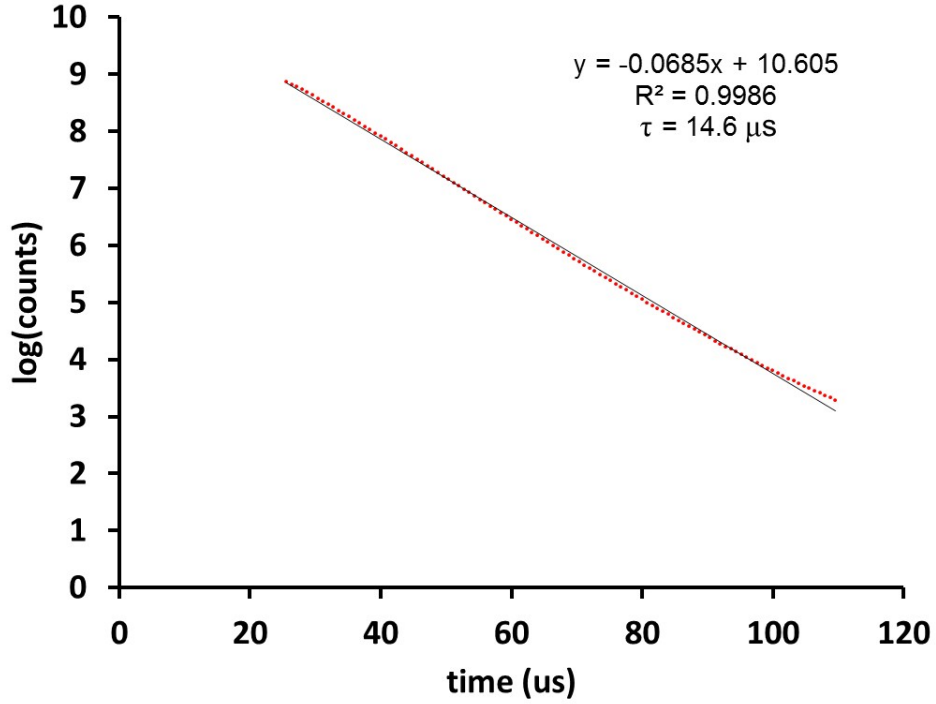

Figure S62. Luminescence decay trace of ($Si^{H}P_2$)Cu(Cbz^{t}^{Bu}) (**2b**) in THF at room temperature.

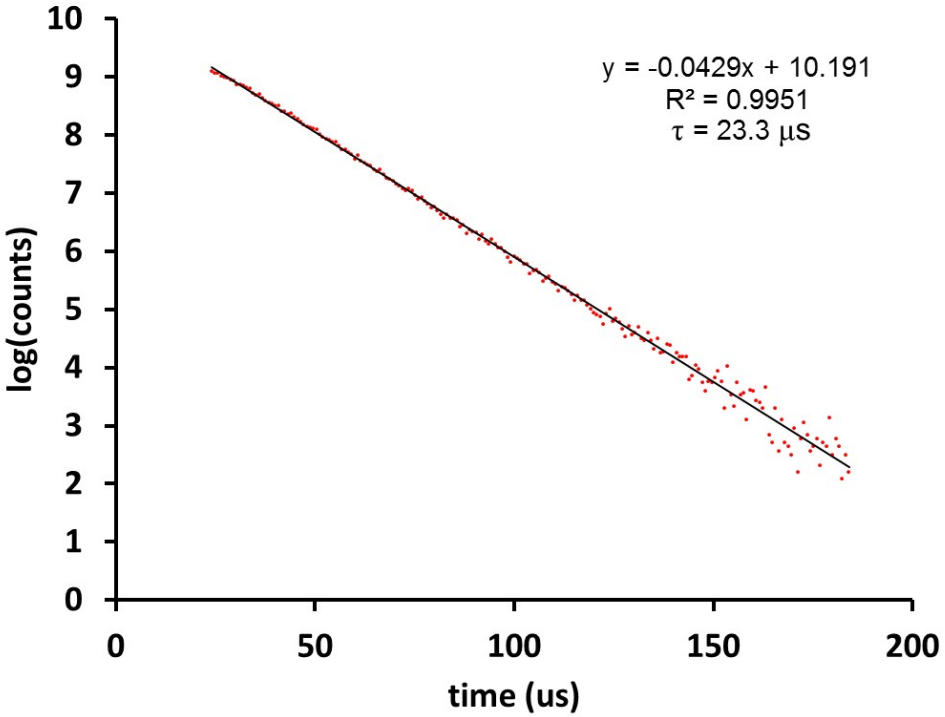

Figure S63. IR spectrum of ($Si^{H}P_2$)CuCl (**1**) (KBr pellet).

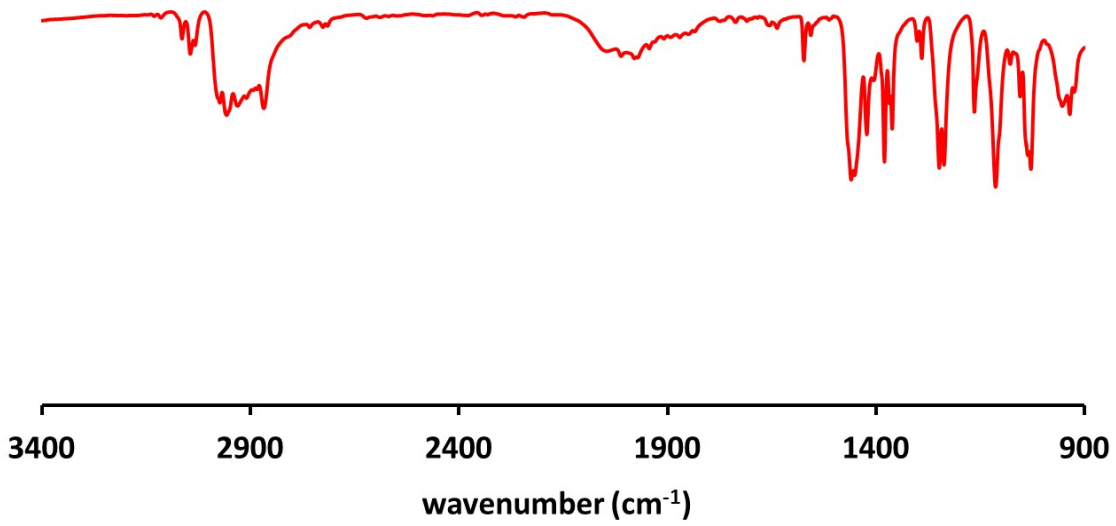

Figure S64. IR spectra of ($Si^{H}P_2$)Cu(Cbz) (**2a**) (blue) and ($Si^{D}P_2$)Cu(Cbz) (**2a-D**) (red) (KBr pellet).

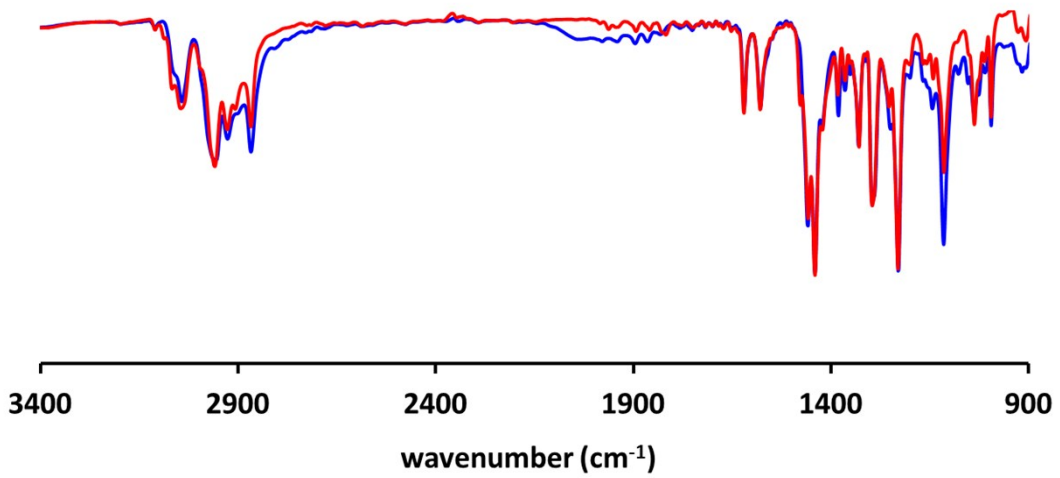

Figure S65. IR spectrum of $(Si^{H}P_2)Cu(Cbz^{tBu})$ (**2b**) (KBr pellet).

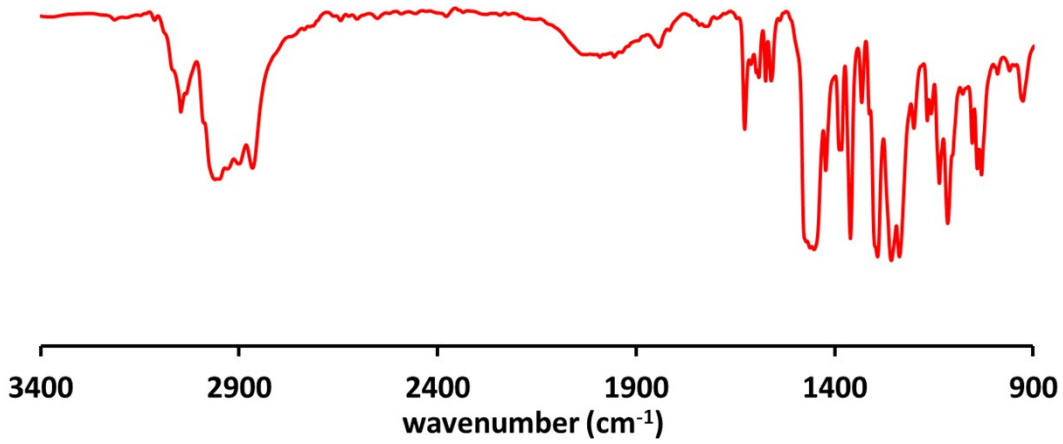

Figure S66. IR spectrum of $(Si^{H}P_2)Cu(Cbz^{I})$ (**2c**) (KBr pellet).

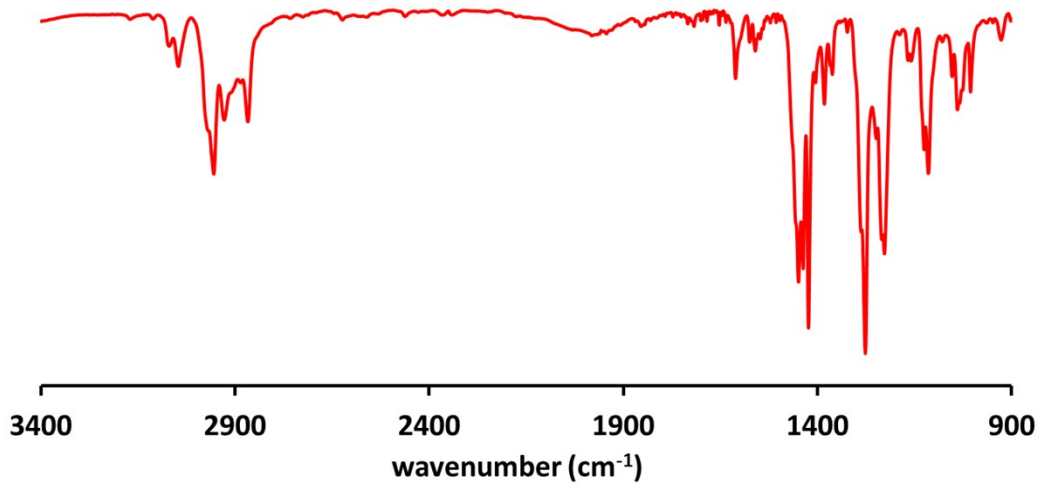

Figure S67. Absorption analyses; (a) experimental spectra (i) and calculated spectra for (ii) **2a**, (iii) **2b** and (iv) **2c** and (b) their TD-DFT calculated electronic transitions with related molecular orbitals relevant to the absorption bands. Color: blue for **2a**, green for **2b** and red for **2c**.

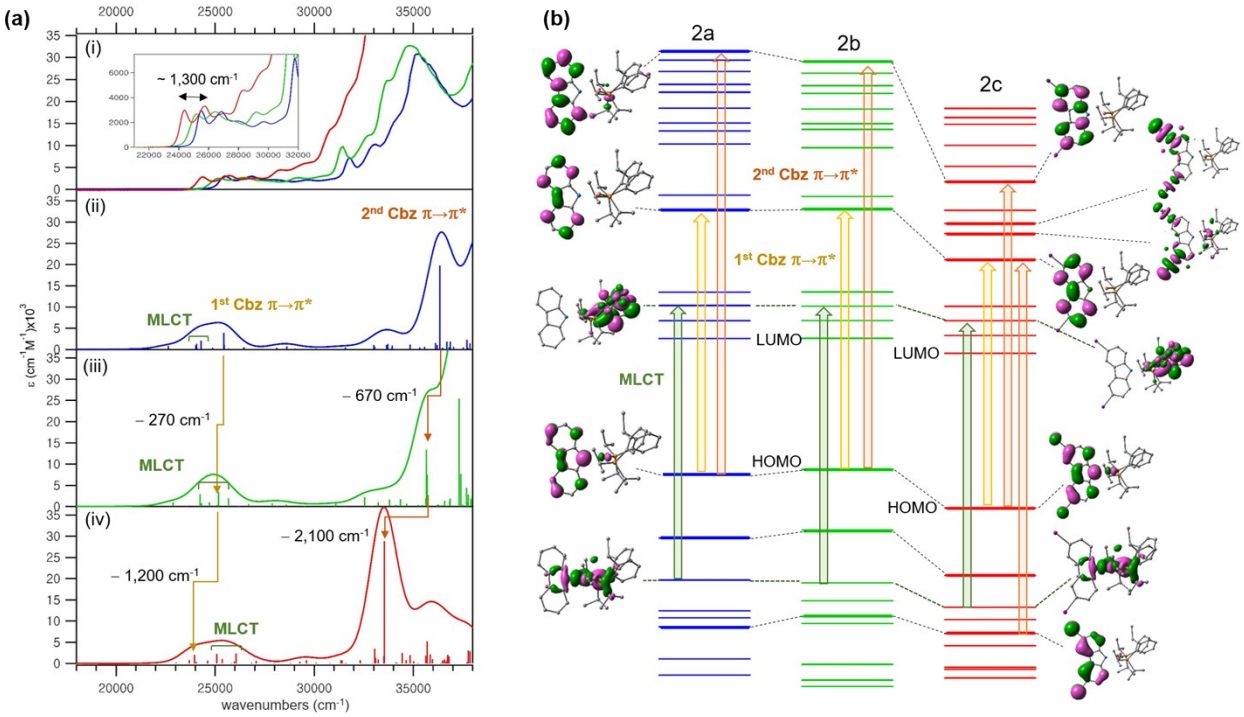

Figure S68. DFT-optimized structure for ($MeSi^{Me}P_2$)Cu(Cbz) showing the effect of missing a Si-H moiety. The Cu-Si (= 4.08 Å), Cu-P2 (= 4.17 Å), Cu-N (= 1.90 Å) and Cu-P1 (= 2.22 Å) distances were obtained.

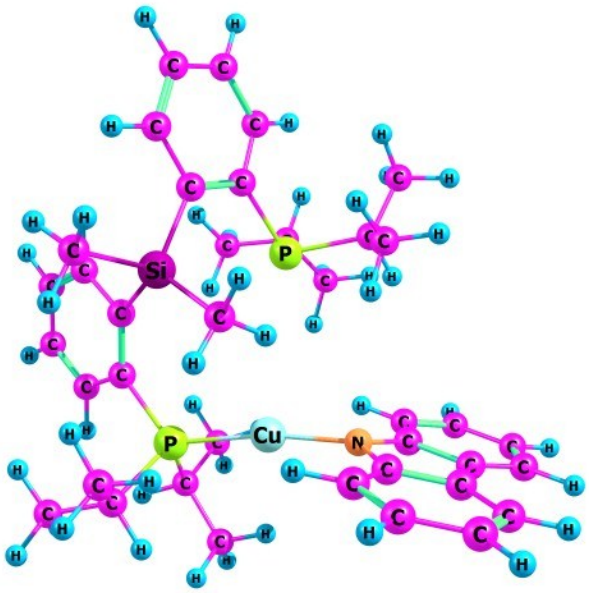

Figure S69. DFT-optimized structures of ($Si^{H}P_2$)Cu(Cbz) (**2a**) (red), deprotonated **2a** (green) and ($PP^{Me}P$)Cu(Cbz) (**4a**) (blue). The structure of deprotonated **2a** is nicely overlaid with that of **4a**.

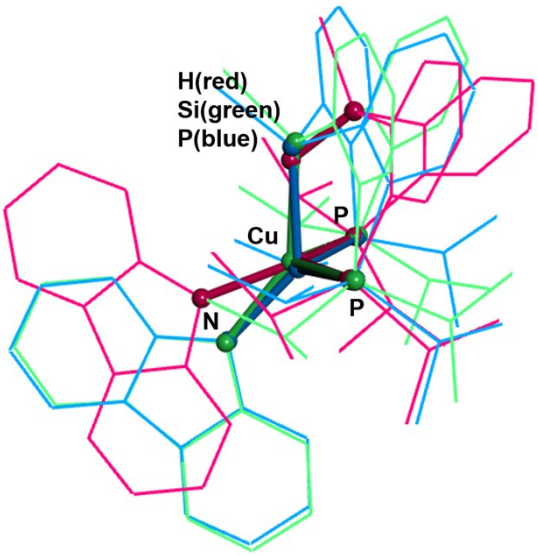

Figure S70. (a) Experimental and (b) TD-DFT-predicted absorption spectra of ($Si^{H}P_2$)Cu(Cbz) (**2a**) (red) and ($PP^{Me}P$)Cu(Cbz) (**4a**) (blue). Excitation wavelengths for emission measurements (a) and major electronic transitions in consideration (b) are denoted with arrows.

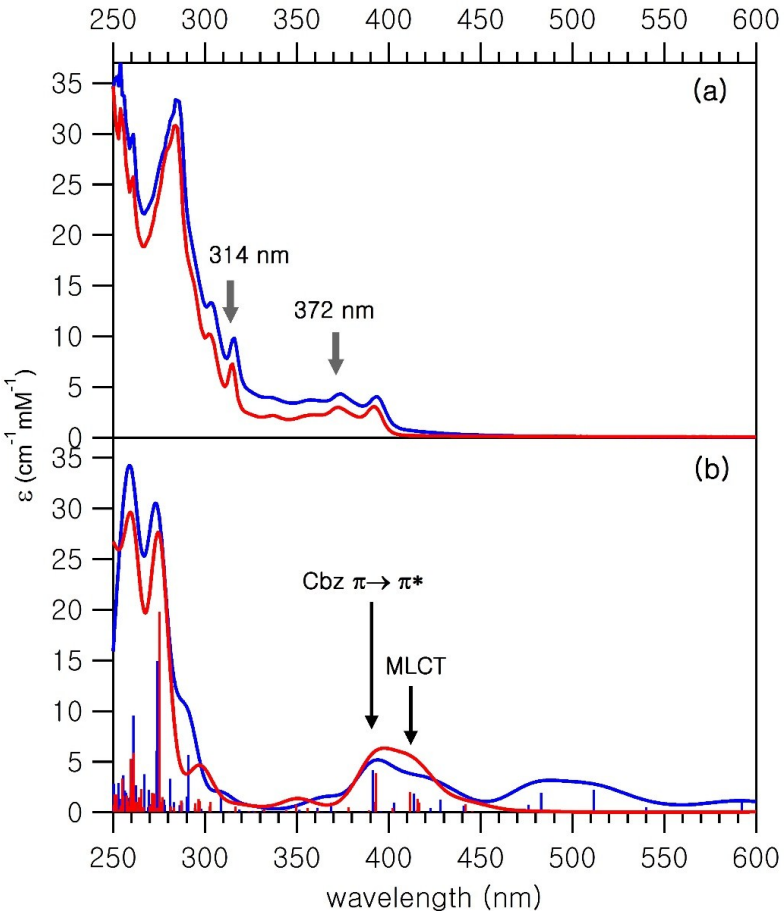

Figure S71. TD-DFT-calculated electronic transitions relevant to the absorption band at 350~400 nm in Figure S50a and the molecular orbitals of ($PP^{Me}P$)Cu(Cbz) (**4a**) (left) and ($Si^{H}P_2$)Cu(Cbz) (**2a**) (right). The #170 and #171 of **4a** correspond to the #172 and #171 of **2a**, respectively, with a variation in the orientation of the Cu-Cbz bond, which lies in the xy plane in **2a** but moves out of the plane in **4a**. The MLCT excited states accessible in this study originate from the transitions from the boxed Cu d-based orbitals to the ligand-based orbitals (green arrows).

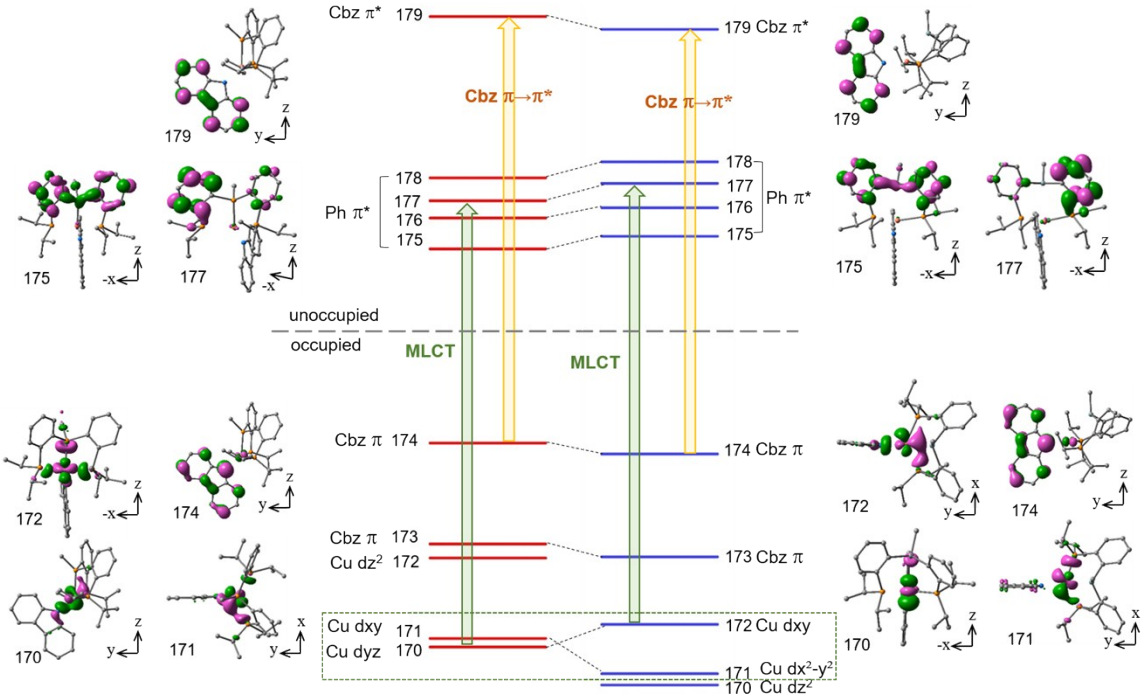

Figure S72. DFT-optimized structures for the singlet (left) and triplet (middle) states of (a) ($PP^{Me}P$)Cu(Cbz) (**4a**) and (b) ($Si^{H}P_2$)Cu(Cbz) (**2a**). The bond lengths of the Cu-ligands are given to the right-hand side. In both complexes, relative to the singlet ground states, the triplet states have electron density shifted from the highest-energy Cu d-based orbitals (#172's in Figure S62) to the phenyl-based orbitals (#175's in Figure S62). This electron density transfer involves a significant change in coordination geometry for **4a**, converting the four-coordinate structure to a pseudo-three-coordinate structure. Alternatively, **2a** undergoes negligible structural changes as expected on basis of Bourissou's study.[25]

(a)

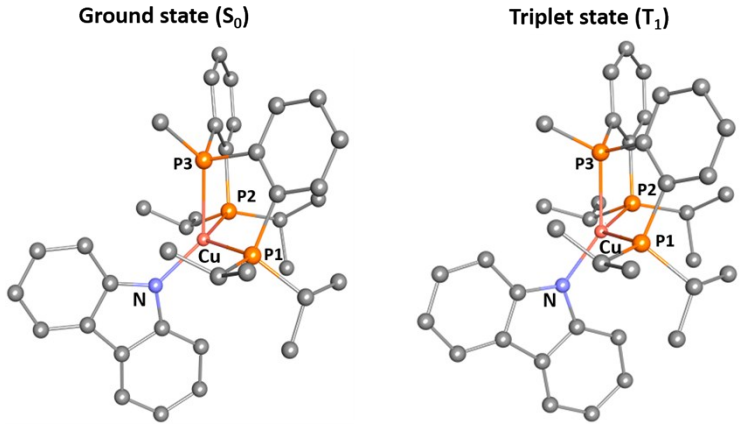

	Singlet	Triplet
Cu-N	2.00 Å	1.99 Å
Cu-P1	2.40 Å	2.40 Å
Cu-P2	2.47 Å	2.65 Å
Cu-P3	2.34 Å	2.34 Å

(b)

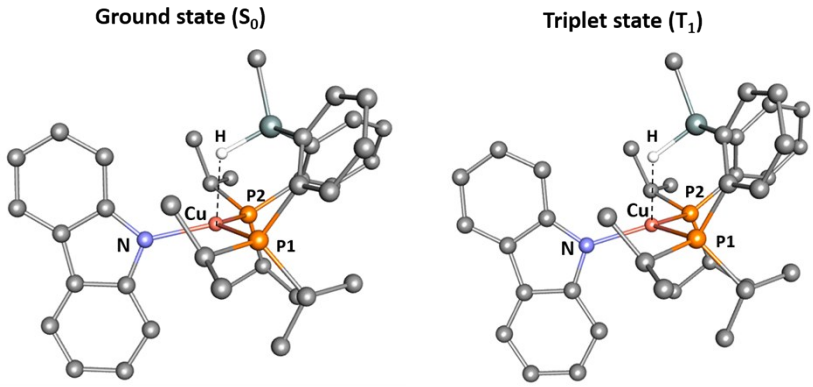

	Singlet	Triplet
Cu-N	2.00 Å	1.98 Å
Cu-P1	2.38 Å	2.42 Å
Cu-P2	2.32 Å	2.36 Å
Cu-H	1.96 Å	1.98 Å

Figure S73. Potential energy curves along the Cu-P2 stretch normal mode of (PP^{Me}P)Cu(Cbz) (**4a**) for the ground state (black open circles and solid curve) and the excited states associated with the MLCT transitions of #171→#177 (red circles), #170→#177 (yellow circles), #171→#178 (green triangles), and #170→#178 (blue triangles) and the Cbz-based π→π* transition (#174→#179; magenta open circles and dashed curve). The #170→#177 and #174→#179 transitions give rise to the absorption band with a prominent intensity in Figure S50a, while the emission band in Figure S50b is attributed only to the excited state associated with the #174→#179 transition. The lack of an emission band from the excited states associated with the MLCT transitions is due to non-radiative relaxation caused by vibronic coupling between the excited states involving contributions from Cu d_{yz}- and Cu d_{xy}-based orbitals (#170 and 171 in Figure S62), which are almost degenerate in the ground state geometry (split by ~400 cm^{-1}, dotted green box at x ~0%) but lifted in the MLCT excited state (split by ~1200 cm^{-1}, dotted green box at x ~40%). The x axis is expressed in the ratio of Cartesian coordinate displacement relative to the normal mode.

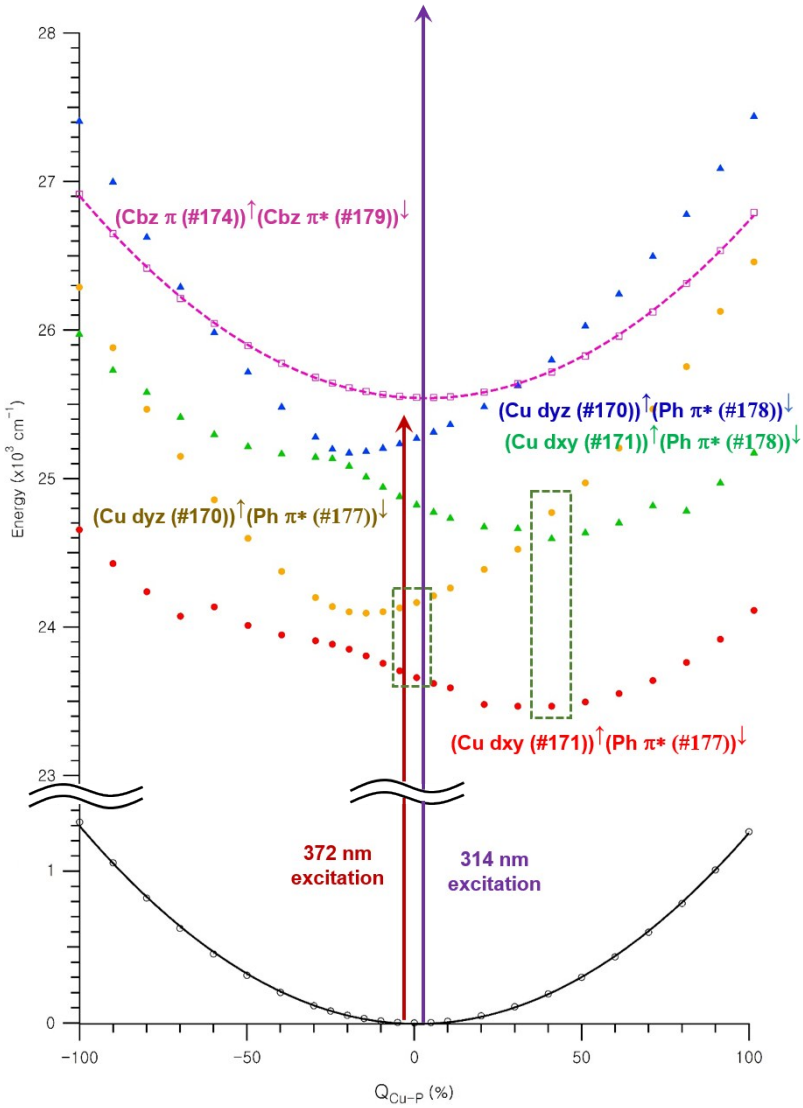

Figure S74. Potential energy curves along the Cu-P2 stretch normal mode of ($Si^{H}P_2$)Cu(Cbz) (**2a**) for the ground state (black open circles and solid curve), the singlet excited states associated with the MLCT transitions (solid colored curves) and the Cbz-based π→π* transitions (dashed colored curves). In contrast to the case of ($PP^{Me}P$)Cu(Cbz) (**4a**), the relevant Cu d orbitals stay split in energy by ~1450 cm^{-1} and thus the MLCT excited states (red and purple curves) do not vibronically couple to each other. Therefore, a population at these excited states can undergo radiative relaxation, resulting the emission band at ~360 nm from the Cbz LC excited state and the band at ~490 nm from the MLCT excited states. Importantly, the singlet excited state of $(\#172)^1(\#177)^1$ lies ~1570 cm^{-1} (~0.19 eV) above its corresponding triplet state, which can participate in the TADF process.

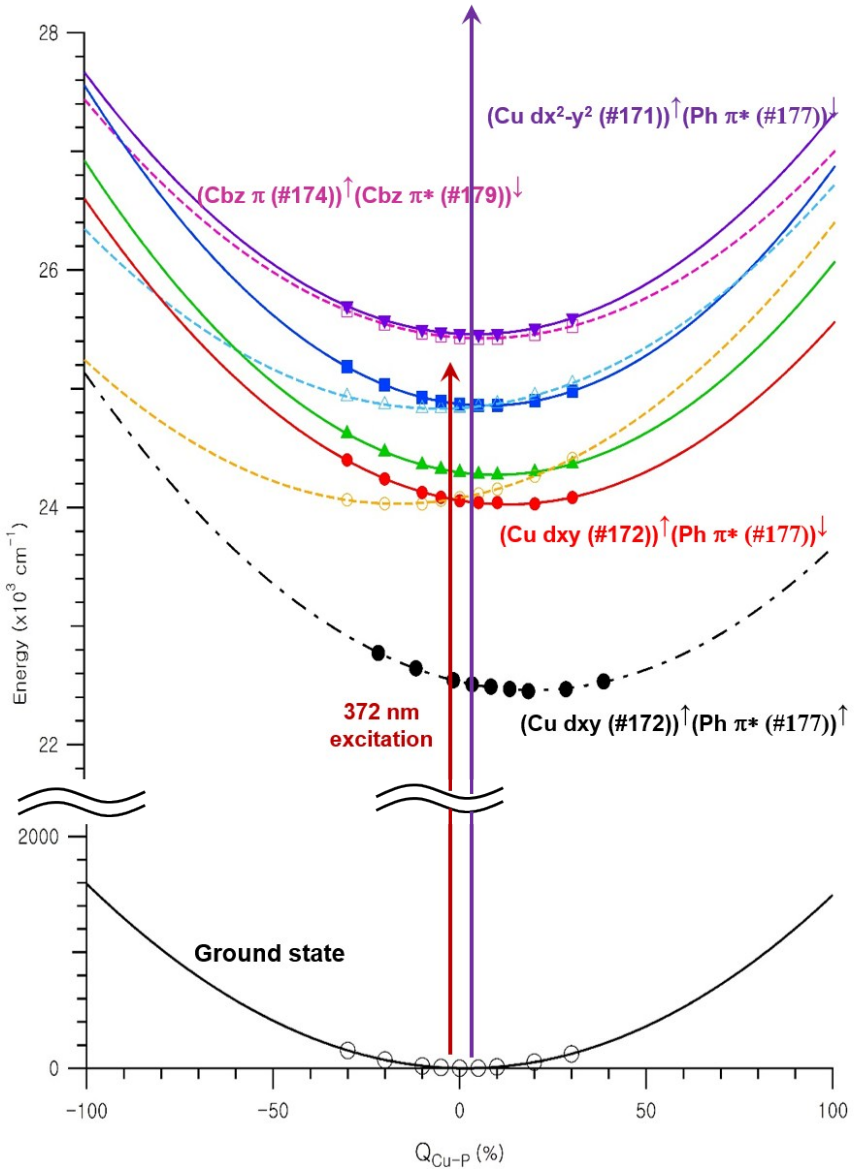

Figure S75. Absorption spectra of ($Si^{H}P_2$)Cu(Cbz) (**2a**) obtained from (a) experiment, (b) TD-DFT computations using the B3LYP functional and (c) the BP86 functional.

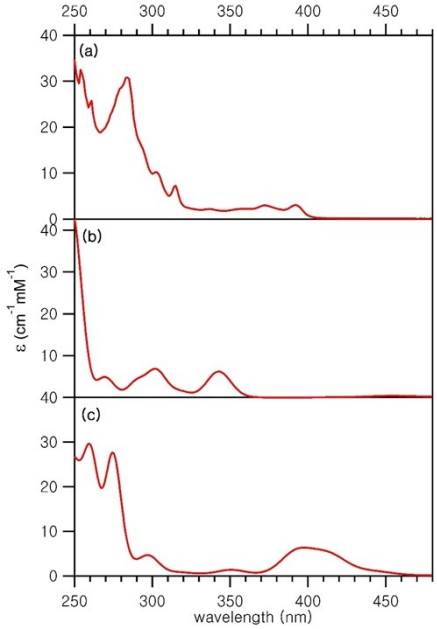

Figure S76. Absorption spectra of ($Si^{H}P_2$)Cu(Cbz) (**2a**) (red) and ($PP^{Me}P$)Cu(Cbz) (**4a**) (blue) obtained from (a) experiment, (b) TD-DFT computations using the def2-SVP and (c) def2-TZVP basis sets.

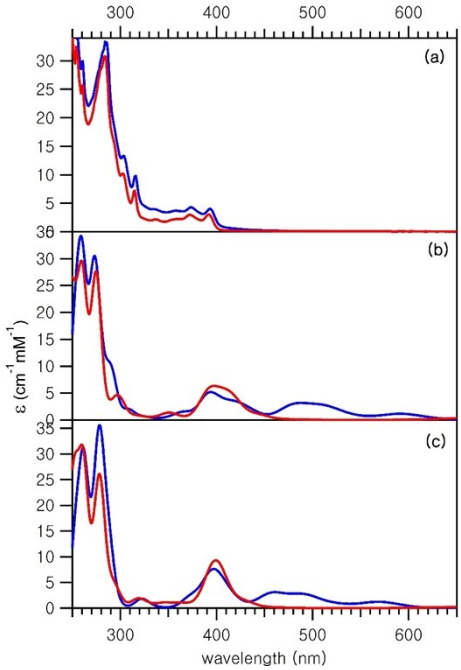

References

1. Y.-E. Kim, J. Kim and Y. Lee, *Chem. Commun.*, 2014, **50**, 11458.
2. H. Fang, Y.-K. Choe, Y. Li and S. Shimada, *Chem. Asian. J.*, 2011, **6**, 2512.
3. J. Kim, Y. Kim, I. Sinha, K. Park, S. H. Kim and Y. Lee, *Chem. Commun.*, 2016, **52**, 9367.
4. *SMART*, Data collection software; Bruker AXS, Inc.: Madison, WI, 2012.
5. *SAINT*, Data integration software; Bruker AXS, Inc.: Madison, WI, 2012.
6. G. M. Sheldrick, SADABS: Program for absorption correction with the Bruker SMART system, Universitat Gottingen, Germany, 1996.
7. G. M. Sheldrick, SHELXTL, *version* 6.1; Bruker AXS, Inc., Madison, WI, 2000.
8. R. J. Abraham and H. J. Bernstein, *Can. J. Chem.*, 1961, **39**, 216.
9. D. A. Redfield, J. H. Nelson and L. W. Cary, *Inorg. Nucl. Chem. Lett.*, 1974, **10**, 727.
10. F. Neese, *WIREs Comput. Mol. Sci.*, 2012, **2**, 73.
11. J. P. Perdew, *Phys. Rev. B*, 1986, **33**, 8822.
12. J. P. Perdew, *Phys. Rev. B*, 1986, **34**, 7406.
13. A. D. Becke, *Phys. Rev. A*, 1988, **38**, 3098.
14. F. Weigend and R. Ahlrichs, *Phys. Chem. Chem. Phys.*, 2005, **7**, 3297.
15. A. Hellweg, C. Hättig, S. Höfener and W. Klopper, *Theor. Chem. Acc.*, 2007, **117**, 587.
16. A. Schäfer, C. Huber and R. Ahlrichs, *J. Chem. Phys.*, 1994, **100**, 5829.
17. A. D. Becke, *J. Chem. Phys.*, 1993, **98**, 5648.
18. C. Lee, W. Yang and R. G. Parr, *Phys. Rev. B*, 1988, **37**, 785.
19. S. H. Vosko, L. Wilk and M. Nusair, *Can. J. Phys.*, 1980, **58**, 1200.
20. A. L. Fetter and J. D. Walecka in *Quantum Theory of Many-particle Systems*, McGraw–Hill, New York, 1971.
21. Due to its poor solubility in benzene, THF-d_8 was utilized for measuring ^{13}C NMR spectrum.
22. D. R. Lide in *CRC Handbook of Chemistry and Physics, 84th Edition*, CRC Press, New York, 2003.
23. J. N. Demas and G. A. Crosby, *J. Phys. Chem.*, 1971, **75**, 991.
24. W. R. Dawson and M. W. Windsor, *J. Phys. Chem.*, 1968, **72**, 3251.
25. M. Joost, S. Mallet-Ladeira, K. Miqueu, A. Amgoune and D. Bourissou, *Organometallics*, 2013, **32**, 898.